Biophysical Properties of Connexin-45 Gap Junction Hemichannels Studied in Vertebrate Cells

Virginijus Valiunas

Department of Physiology and Biophysics, State University of New York at Stony Brook, Stony Brook, NY 11794

ABSTRACT Human HeLa cells transfected with mouse Cx45 and rat RIN cells transfected with chicken Cx45 were used to study the electrical and permeability properties of Cx45 gap junction hemichannels. With no extracellular Ca^{2+}, whole-cell recording revealed currents arising from hemichannels in both transfected cell lines. Multichannel currents showed a time-dependent activation or deactivation sensitive to voltage, V_m. These currents did not occur in nontransfected cells. The hemichannel currents were inhibited by raising extracellular Ca^{2+} or by acidification with CO_2. The unitary conductance exhibited V_m dependence (i.e., $\gamma_{hc,main}$ increased/decreased with hyperpolarization/depolarization). Extrapolation to $V_m = 0$ mV led to a $\gamma_{hc,main}$ of 57 pS, roughly twice the conductance of an intact Cx45 gap junction channel. The open channel probability, P_o, was V_m-dependent, declining at negative V_m ($P_o < 0.11$, $V_m < -50$ mV), and increasing at positive V_m ($P_o \sim 0.76$, $V_m > 50$ mV). Moreover, Cx45 nonjunctional hemichannels appeared to mediate lucifer yellow (LY) and propidium iodide (PI) dye uptake from the external solution when extracellular Ca^{2+} level was reduced. Dye uptake was directly proportional to the number of functioning hemichannels. No significant dye uptake was detected in nontransfected cells. Cx45 transfected HeLa and RIN cells also allowed dye to leak out when preloaded with LY and then incubated in Ca^{2+}-free external solution, whereas little or no dye leakage was observed when these cells were incubated with 2 mM external Ca^{2+}. Intact Cx45 gap junction channels allowed passage of either LY or PI dye, but their respective flux rates were different. Comparison of LY diffusion through Cx45 hemichannels and intact gap junction channels revealed that the former is more permeable, suggesting that gap junction channel pores exhibit more allosterical restriction to the dye molecules than the unopposed hemichannel. The data demonstrate the opening of Cx45 nonjunctional hemichannels in vertebrate cells when the external Ca^{2+} concentration is reduced.

KEY WORDS: connexins • electrophysiology • intercellular communication • hemichannel • perm-selectivity

INTRODUCTION

Intercellular communication is mediated via conduction and/or diffusion through gap junction channels. Gap junctions constitute assemblies of intercellular channels. Each channel consists of two hemichannels (connexons) composed of six transmembrane proteins (connexins). Each intercellular channel provides an aqueous pathway for the passage of intracellular ions and small molecules. It has been demonstrated that gap junction channels are permeable to ions, fluorescent dyes, and physiologically active molecules including amino acids, second messengers, and small peptides (Bevans et al., 1998; Saez et al., 1989; Vaney et al., 1998). To date, at least 19 connexins have been identified in vertebrate cells encoded by a multigene family (Bruzzone et al., 1996; Beyer and Willecke, 2000). An interesting aspect of the various gap junctions is their apparent differences in terms of perm-selectivity (molecular permeability and ion selectivity). It has been shown that Cx40, Cx43, and Cx37 gap junction channels each have a unique selectivity pattern for cations and anions (Beblo and Veenstra, 1997; Wang and Veenstra, 1997). Moreover, the permeability to negatively charged dyes of each these gap junction channels appears to be different (Veenstra et al., 1995).

Oligomerization of connexins into hemichannels occurs before entry into the Golgi apparatus (Evans et al., 1999). Docking of two hemichannels to form a gap junction channel involves noncovalent interactions (Foote et al., 1998) and results in the formation of leak-free intercellular channel (Bukauskas et al., 1995a). Hemichannels in nonjunctional membrane areas can gate open under appropriate conditions. Evidence for the existence of nonjunctional hemichannels was first provided by electrical studies on horizontal cells of fish retina (De Vries and Schwartz, 1992; Malchow et al., 1993). Similar observations were subsequently made in *Xenopus* oocytes exogenously expressing known connexins. Injection of mRNA for rat Cx46 or chicken Cx56 induced currents attributable to hemichannels (Ebihara and Steiner, 1993; Ebihara et al., 1995). Later, it was shown that Cx38, the intrinsic connexin of *Xenopus* oocytes, also forms hemichannels (Ebihara, 1996). It also has been demon-

V. Valiunas is on leave from Institute for Biomedical Research, Kaunas Medical University, Eiveniu 4 LT-3007 Kaunas, Lithuania.

Address correspondence to Virginijus Valiunas, Department of Physiology and Biophysics, Health Science Center, State University of New York at Stony Brook, Stony Brook, NY 11794-8661. Fax: (631) 444-3432. E-mail: virgis@mail.pnb.sunysb.edu

strated that injected *Xenopus* oocytes are suitable to study single hemichannels (Trexler et al., 1996).

Under pathophysiological conditions, like ischemia or other forms of metabolic insult, rapid disturbances in ionic homeostasis contribute to cellular injury and death (Wilde and Aksnes, 1995). The physiological role of nonjunctional hemichannels remains to be identified, but the hemichannel activity has been reported to be controlled by the extracellular Ca^{2+} (Ebihara and Steiner, 1993; Pfahnl and Dahl, 1999; Valiunas and Weingart, 2000), the metabolic state (John et al., 1999), the membrane potential (De Vries and Schwartz, 1992; Ebihara et al., 1995; Trexler et al., 1996; Valiunas and Weingart, 2000), and Ca^{2+}-dependent volume regulation (Quist et al., 2000). Conceivably, nonjunctional hemichannels also may be involved in the pathogenesis of ionic disturbances during myocardial ischemia and hypoxia. However, little is known about the properties of cardiac nonjunctional hemichannels.

This study was concentrated on the properties of Cx45 hemichannels. Cx45 is one of the three major connexins expressed in heart. It has been reported to be widely distributed in myocytes of different types of cardiac tissues (working, conductive and nodal; Kanter et al., 1993; Davis et al., 1994; Saffitz et al., 1994; Alcolea et al., 1999; Coppen et al., 1999). Cx45 gap junction channels possess relatively small unitary conductances for gap junction channels (~26 pS), but still are able to pass some dyes (Veenstra et al., 1994a).

The aim of this study was to investigate the electrical and perm-selectivity properties of hemichannels in vertebrate cells. We used human HeLa cells transfected with mouse Cx45 and rat islet tumor (RIN)* cells transfected with chicken Cx45. The main emphasis was on Cx45 hemichannel conductance, gating and permeability and comparison to that of the intact gap junction channel. The study illustrates for the first time that Cx45 is capable of forming operational hemichannels, which are voltage, pH and calcium gated. Moreover, we provide the first characterization of the biophysical properties of Cx45 hemichannels.

MATERIALS AND METHODS

Cells and Culture Conditions

Experiments were performed on human HeLa cells transfected with cDNA coding for mouse Cx45 and rat islet tumor (RIN)* cells transfected with cDNA coding for chicken Cx45. HeLa cells and RIN cells were grown in DME medium and RPMI 1640 medium, respectively, supplemented with 10% FCS, 100 μg/ml streptomycin, and 100 U/ml penicillin. Transfected HeLa cells and RIN cells were selected using 0.5–1 μM puromycin (Sigma-Aldrich) and 0.4 mg/ml G418 (Geneticin; Life Technologies), respectively. The cells were passaged weekly, diluted 1:10, and kept at 37°C in a CO_2 incubator (5% CO_2, 95% ambient air). To perform experiments, the cells were harvested and seeded onto sterile glass coverslips placed in multiwell culture dishes (~10^4 cells/cm^2). Electrophysiological experiments were performed on cells cultured for 1–3 d.

Solutions and Pipettes

During experiments, the cells were superfused with bath solution containing the following (in mM): 120 potassium aspartate, 10 NaCl, 2 $CaCl_2$, 5 HEPES, pH 7.4, 5 glucose, and 2 mM CsCl, $BaCl_2$, and TEA^+ Cl^- were added. For the Ca^{2+}-free (0 Ca^{2+}) bath solution, $CaCl_2$ was omitted. The patch pipettes were filled with solution containing the following (in mM): 120 potassium aspartate, 10 NaCl, 3 MgATP, 5 HEPES, pH 7.2, and 10 EGTA (pCa ~8); filtered through 0.22-μm pores. In perforated patch experiments, the pipette solution contained 30–50 μM β-escin (Fan and Palade, 1998).

Electrical Measurements

Glass coverslips with adherent cells were transferred to an experimental chamber perfused with bath solution at room temperature (~22°C). The chamber was mounted on the stage of an inverted microscope (Olympus IMT2). Patch pipettes were pulled from glass capillaries (code 7052; A-M Systems) with a horizontal puller (Sutter lnstruments). When filled, the resistance of the pipettes measured 1–2 MΩ.

Experiments were performed on single cells using the whole-cell voltage-clamp technique (Valiunas and Weingart, 2000). A selected cell was attached to a patch pipette connected to a micromanipulator (model WR-88; Narishige Scientific Instrument) and an amplifier (model Axopatch 200; Axon Instruments, Inc.). This method permitted control of the membrane potential (V_m), and allowed measurement of the associated membrane current (I_m).

Dual whole-cell patch clamp was used in experiments with cell pairs. It allowed to control the membrane potential of both cells and to measure the currents (Bukauskas et al., 1995b; Brink et al., 1996). Initially, the membrane potential of cell 1 and cell 2 was clamped to the same value, $V_1 = V_2$. V_2 was then changed to establish a transjunctional voltage, $V_j = V_2 - V_1$. Currents recorded from cell 2 represent the sum of two components, the junctional current (I_j) and the membrane current of cell 2 ($I_{m,2}$); the current obtained from cell 1 corresponds to I_j.

Dye-uptake and Dye-injection Studies

Nontransfected (NT) and transfected HeLa or RIN cells were incubated in the bath solution (with 2 mM Ca^{2+} or Ca^{2+} free) containing 1 mg/ml lucifer yellow (LY; Molecular Probes) or 2 mg/ml propidium iodide (PI; Molecular Probes) for 30 min at room temperature (22°C).

The dye transfer through gap junctions was investigated using cell pairs. Dyes were dissolved in pipette solution to reach a concentration 0.1% for LY and 0.2% for PI. In each cell pair examined, the whole-cell recording mode was established on one cell with a dye-filled pipette. The second cell was patched either in the perforated-patch mode or a gigaohm seal was established with the pipette leaving the patch intact. This allowed the dye to spread into the recipient cell. Once dye had spread, the whole-cell recording mode also was established in the recipient cell and the gap junction conductance (g_j) was measured. This procedure and the perforated patch method allowed the dye to spread to the neighboring cell without loss of dye caused by patch pipette dialysis and to measure simultaneously g_j.

**Abbreviations used in this paper:* NT, nontransfected; LY, lucifer yellow; PI, propidium iodide; P_o, open state probability; RIN, rat islet tumor.

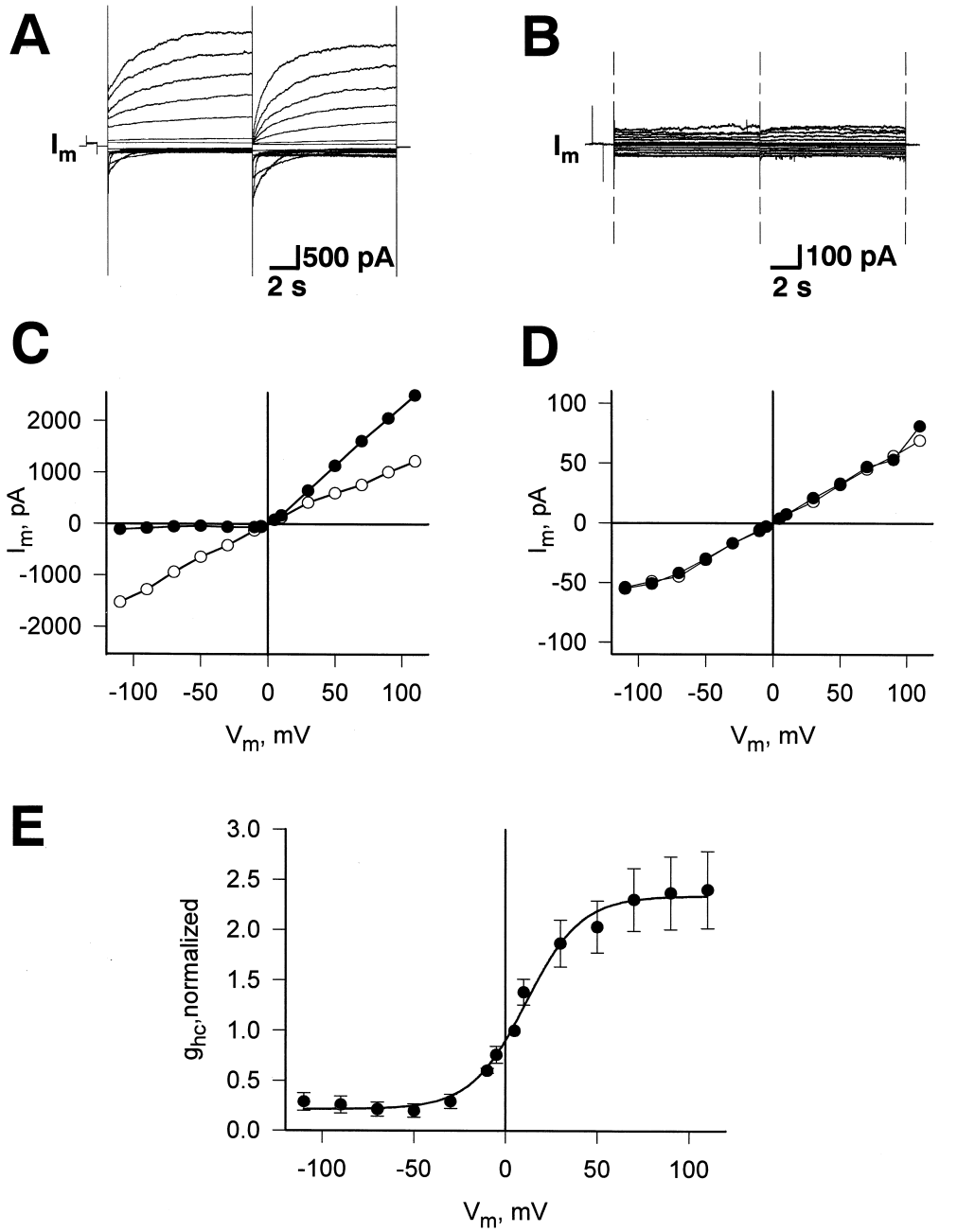

FIGURE 1. (A and B) Currents elicited in a HeLa cell expressing Cx45. Starting from 0 mV, the membrane potential, V_m, was depolarized or hyperpolarized in steps to elicit outward/inward currents, I_m. (A) I_m responses recorded in solution with no added Ca^{2+}. This induced an extra current component with a time-dependent activation or inactivation, attributable to hemichannels. (B) I_m responses recorded in solution with 2 mM Ca^{2+}. C-D Plots of $I_{m,inst}$ (○) and $I_{m,ss}$ (●) versus V_m, determined in a Cx45-HeLa cell with no added Ca^{2+} (C) and with 2 mM Ca^{2+} (D) in bath solution. (E) Dependence of hemichannel conductance at steady state, $g_{hc,ss}$ on voltage, V_m, determined in Cx45-HeLa cells. Symbols correspond to the mean values obtained from five cells. Smooth curve: best fit of data to the Boltzmann equation ($V_{m,0}$ = +11.1 mV, $g_{hc,max}$ = 2.34, $g_{hc,min}$ = 0.21, z = 1.7.

Fluorescent dye uptake and cell-to-cell spread was imaged using a 12-bit 64,000 pixel grayscale digital CCD-camera (model LYNXX 2000T; Spectra Source Instruments).

Signal Recording and Analysis

Voltage and current signals were recorded on chart paper (model Gould RS 2400; Gould Instruments) and videotape (pulse-code modulated DR-384; Neuro Data Instruments). For off-line analysis, the current signals were filtered at 1 kHz, digitized with a 12-bit A/D-converter (model DT21EZ; Data Translation) and stored with a personal computer. Data acquisition and analysis were performed with custom-made software (Brink et al., 1996; Krisciukaitis, 1997). Curve fitting and statistical analyses were done with SigmaPlot and SigmaStat, respectively (Jandel Scientific). The results are presented as means ± SEM.

RESULTS

Hemichannel Currents in Transfected Cells: Modulation by Voltage and External Ca^{2+}

Recordings from HeLa and RIN cells expressing mouse Cx45 and chicken Cx45, respectively, showed slowly activating currents in Ca^{2+}-free bath solution. These currents were absent in cells not expressing Cx45, suggesting they were mediated by Cx45 hemichannels.

Fig. 1 A illustrates the voltage protocol used to activate hemichannel currents. A family of I_m traces were elicited by depolarizing (outward currents) and hyperpolarizing pulses (inward currents). The records were

obtained from a Cx45-HeLa cell superfused with Ca^{2+}-free solution. After establishing of the whole-cell recording conditions, the membrane potential (V_m) was clamped to 0 mV. Bipolar voltage pulses of 10-s duration were then delivered to alter V_m in steps of ±5, ±10, and then to ±110 mV using increments of 20 mV. The associated membrane currents (I_m) increased proportionally with V_m and showed a voltage- and time-dependent activation or deactivation. In the absence of Ca^{2+}, depolarization produced slowly activating outward currents (Fig. 1 A), whereas hyperpolarization induced inward currents which deactivated with time.

Perfusion with 2 mM Ca^{2+} closed the hemichannels in a time-dependent manner. In the presence of 2 mM extracellular Ca^{2+}, the bipolar pulse protocol applied to the same cell elicited small outward and inward currents. These currents increased with depolarization and hyperpolarization, but showed no slow time dependent changes (Fig. 1 B). Thus, the hemichannel activity was suppressed completely in the presence of 2 mM external Ca^{2+}.

These experiments show that membrane currents can be activated in Cx45 expressing cells by lowering Ca^{2+} in the external solution. Similar observations were made in *Xenopus oocytes* (Ebihara et al., 1995; Trexler et al., 1996) and HeLa cells (Valiunas and Weingart, 2000) expressing other connexins. Beside the hemichannels, which opened at 0 mV by lowering of Ca^{2+}, positive voltages cause further activation of hemichannels. In contrast, negative V_m closed the hemichannels previously opened by lowering Ca^{2+} and depolarization.

The signals obtained in Ca^{2+}-free external solution (Fig. 1 A) were analyzed to obtain the relationships $I_m = f(V_m)$. The amplitudes of I_m were determined at the beginning ($I_{m,inst}$; inst, instananeous) and end of each pulse ($I_{m,ss}$; ss, steady state). To distinguish between capacitive and ionic currents at the beginning of each record, the signals were displayed at fast time resolution. At large negative voltages, $I_{m,inst}$ was determined by fitting the inward current with an exponential. As shown in Fig. 1 C, $I_{m,inst} = f(V_m)$ (○) was slightly nonlinear over the voltage range examined (i.e., ±110 mV). The $I_{m,inst}$ was ~20% larger at −110 mV in comparison to the current at +110 mV. In contrast, $I_{m,ss} = f(V_m)$ (●) deviated strongly from linearity. It was shallower at negative V_m and steeper at positive V_m. Fig. 1 D shows the $I_m = f(V_m)$ relationship recorded in the presence of 2 mM extracellular Ca^{2+}. The instantaneous (Fig. 1 D, ○) and steady-state currents (Fig. 1 D, ●) were virtually linear and superimposable. The analysis yielded a uniform slope conductance of 0.6 nS.

The presence 2 mM Cs^+, Ba^{2+}, or TEA^+ in the extracellular and intracellular solution does not block the novel current seen in Ca^{2+}-free solution, suggesting that the Ca^{2+}-sensitive I_m reflects current through hemichannels, I_{hc} (hc, hemichannel). Similar results were obtained from RIN cells transfected with chicken Cx45 (unpublished data).

Voltage Dependence of Hemichannel Currents

The relationship between V_m and g_{hc} was studied in Ca^{2+}-free solution using the bipolar pulse protocol. The signals in Fig. 1 A and others were analyzed to determine the voltage dependence of I_{hc}. Fig. 1 E summarizes the data gathered from five cells. The normalized steady-state conductance ($g_{hc,ss}$) values were calculated from the ratios $I_{hc,ss}/V_m$, normalized with respect to the value at $V_m = +5$ mV, were averaged, and plotted versus V_m. The $g_{hc,ss}$ decreased in a sigmoidal manner to $g_{hc,min}$ when V_m was made negative and increased to $g_{hc,max}$ at positive voltages. The smooth curve represents the best fit of data to the Boltzmann equation:

$$g_{hc,\,ss} = \frac{g_{hc,\,\max} - g_{hc,\,\min}}{1 + e^{[A\cdot(V_m - V_{m,\,0})]}} + g_{hc,\,\min},$$

where $g_{hc,max}$ and $g_{hc,min}$ are the maximal and minimal conductance at large positive and negative V_m, respectively. $V_{m,0}$ corresponds to V_m at which $g_{hc,ss}$ is half maximally inactivated. A is a constant which expresses gating charge, $zq(kT)^{-1}$, where z is the equivalent number of unitary positive charges, q moving through the applied electric field, and k and T are the Boltzmann constant and the temperature in Kelvin, respectively. The analysis yielded the following values: $V_{m,0} = 11.1$ mV, $g_{hc,max} = 2.34$, $g_{hc,min} = 0.21$, and $z = 1.7$. The relationship in Fig. 1 E resembles the negative limb of the function $g_{j,ss} = f(V_j)$ of gap junctions studied in cell pairs (Valiunas et al., 2000).

The value of $g_{hc,inst}$ determined at the beginning of a depolarizing pulse reflects the sum of the conductances of the hemichannels opened by the reduction of the extracellular Ca^{2+}. In the case of Cx45-HeLa cells, $g_{hc,inst}$ averaged 6.54 ± 1.1 nS ($n = 19$); in the case of Cx45-RIN cells, $g_{hc,inst}$ averaged 1.72 ± 0.52 nS ($n = 8$). This suggests that the level of connexin expression is ~3.8-fold larger in HeLa cells than in RIN cells.

Assuming that endogenous membrane channels are involved, the value of $g_{hc,inst}$ has to be corrected by subtraction of membrane leak conductance (~0.6 nS, Fig. 1 D). Hence, the corrected $g_{hc,inst}$ for the Cx45-HeLa cells would be ~5.94 nS.

Acidification Affects Macroscopic Hemichannel Currents

Exposure to 100% CO_2 reduces the gap junction conductance (g_j) via lowering of the pH_i (Bukauskas and Peracchia, 1997). Trexler et al. (1999) have shown that this intervention reduces the macroscopic currents through Cx46 hemichannels in *Xenopus oocytes*. The effects of acidification on macroscopic hemichannel cur-

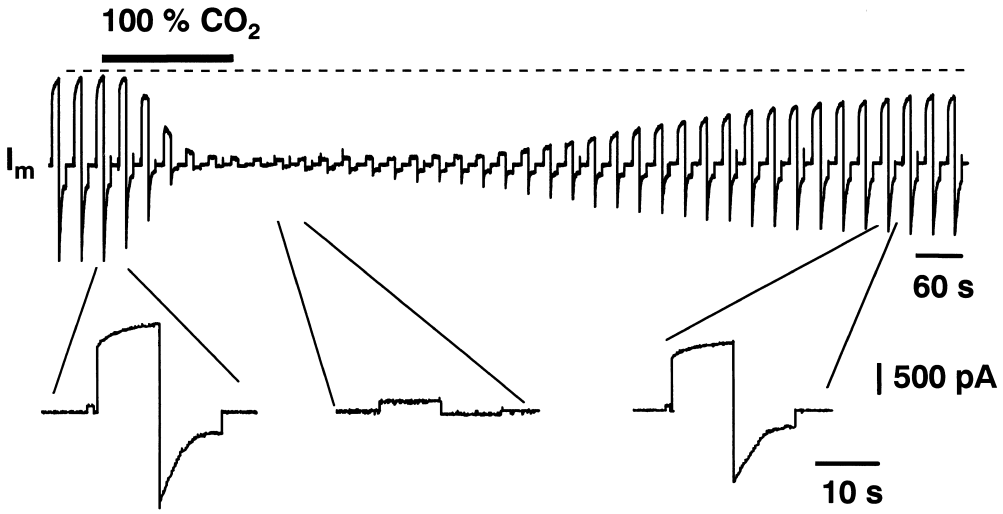

FIGURE 2. Regulation of hemichannel currents by acidification. Hemichannel currents were deactivated by CO_2 and activated during washout.

rents were studied in Cx45-HeLa cells. Fig. 2 illustrates the effects of 100% CO_2 on I_m (I_{hc}). Hemichannel currents were activated and deactivated by bipolar pulses (±50 mV, 10-s duration each) starting from a holding potential of 0 mV. The bipolar pulses were repeated every 10 s. After a 2-min control, perfusion with bath solution equilibrated with 100% CO_2 was started. This led to a gradual decrease in I_{hc} (Fig. 2, continuous current trace and insets). After ~160 s, the slowly activating/deactivating outward/inward I_{hc} were completely abolished. Depolarization and hyperpolarization exhibited small constant currents similar to those seen in NT HeLa cells (Valiunas and Weingart, 2000) or in Cx45-HeLa cells in the presence of 2 mM external Ca^{2+} (Fig. 1 B). Washout of CO_2 led to a gradually recovery of I_{hc}; 13.5 min later the recovery was 75% complete. Similar results were obtained in five other cells.

Multichannel versus Single-channel Currents

Transfected HeLa cells and RIN cells often showed I_{hc} signals from tens of hemichannels. They were used to examine multichannel currents. Fig. 3 compares multichannel and single-channel currents through hemichannels. The cell was superfused with Ca^{2+}-free solution. Fig. 3 A shows multichannel currents elicited by biphasic pulse (±50 mV; top trace). Depolarization gave rise to a time-dependent increase in I_{hc} exhibiting discrete current steps. About 9–10 hemichannels were involved during this episode. Hyperpolarization led to a large $I_{hc,inst}$ which decreased rapidly to a level attributable to endogenous channels. With this time resolution no discrete current steps could be resolved.

Fig. 3 B shows a current signal displayed at higher magnification, evoked by depolarization of 30 mV (top trace). After a capacitive spike, I_{hc} revealed discrete steps indicating the sequential opening and closing of hemichannels (channel opening: upward deflections). The smooth curve on the right-hand side represents an all-point histogram of the current trace. It suggests the involvement of three to four hemichannels. The distances between the peaks were 1.53, 1.48, and 1.54 pA. Hence, the current steps were of comparable amplitudes and correspond to conductance steps of ~49–51 pS.

Deactivation of I_{hc} associated with hyperpolarization appears to be much faster than activation. Fig. 3 C shows a current signal displayed at high magnification induced by hyperpolarization from 50 to −50 mV (Fig. 3 C, top trace). At the beginning of the episode, V_m was at 50 mV. The outward I_{hc} showed discrete steps indicative of hemichannels. The following hyperpolarization to −50 mV led to an inward I_{hc} that deactivated quickly. Discrete steps indicative of sequential closure of hemichannels could now be resolved (channel closure: upward deflections). The analysis of the current peaks yielded conductance steps of 65–73 pS.

Hence, the time-dependent increase/decrease of I_{hc} associated with depolarization/hyperpolarization shown in Fig. 3 (A–C) is caused by activation/deactivation of hemichannels, whose single-channel conductance for inward current is somewhat higher than for outward current.

Single Hemichannel Activity in the Cell-attached Mode

The data presented so far were obtained in the whole-cell recording mode. The advantage of this method is that it allows us study of multichannel and single-channel currents. However, data also have been collected in the cell-attached patch mode, a method suitable to analyze single-channel currents. At the end of an experiment, the membrane patch was disrupted and V_m of ~0 mV was recorded, so the voltage across the membrane patch, V essentially equals $-V_{pip.}$

Fig. 3 (D–F) illustrate records of one operational channel obtained from cells at different voltages.

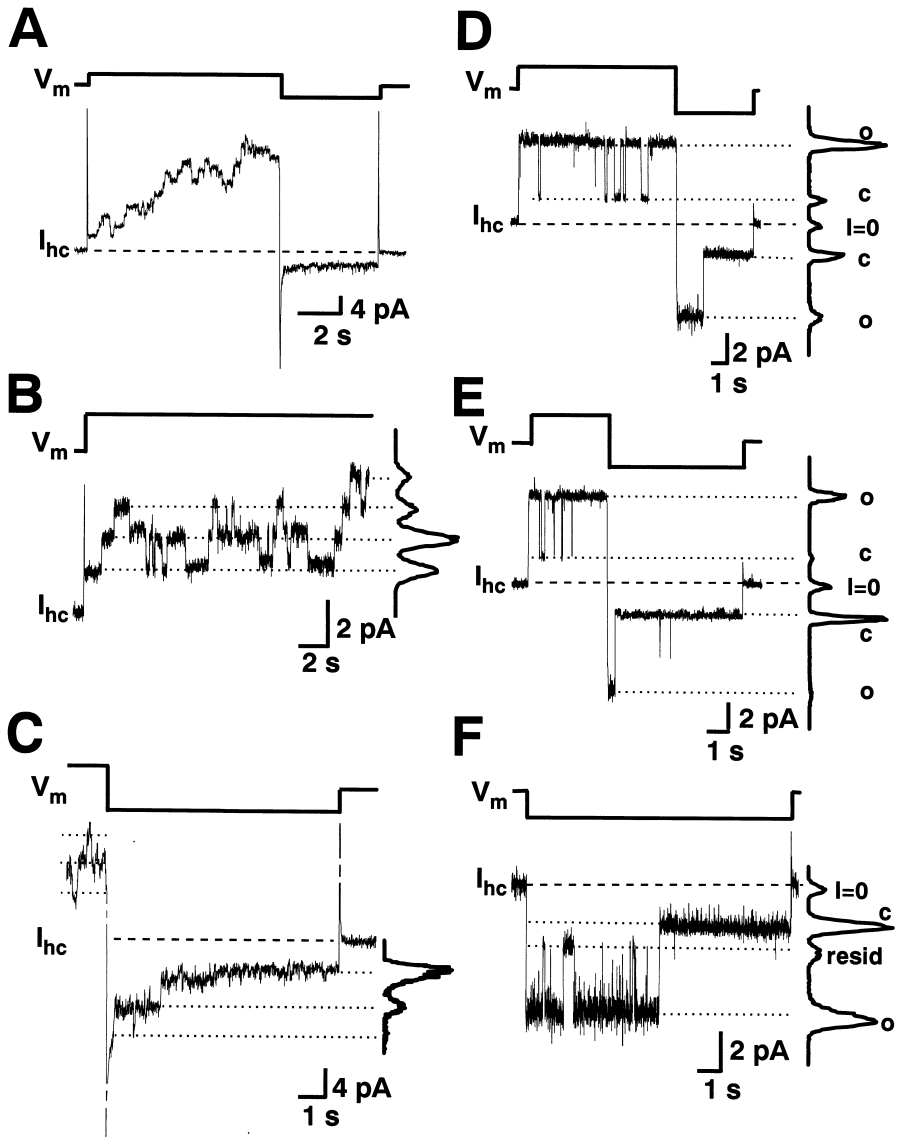

FIGURE 3. Multi versus single hemichannel currents, I_{hc}, recorded from Cx45-HeLa cell with no Ca^{2+} added to the bath. (A) Multichannel I_{hc}, elicited by symmetrical biphasic 50 mV pulses from a holding potential of 0 mV. (B) Single-channel I_{hc} (bottom trace), elicited by depolarization from 0 to 30 mV (top trace). I_{hc} shows discrete steps indicative of opening and closing of hemichannels. The current steps yielded a conductance of ~49–51 pS. (C) Single-channel I_{hc} (bottom trace), induced by hyperpolarization from +50 to −50 mV (top trace). I_{hc} showed discrete steps indicative of sequential closure of hemichannels. The current histograms yielded a conductance of 65–73 pS. (D–F) Hemichannel currents, I_{hc}, from a Cx45-HeLa cell, recorded in the cell-attached patch configuration. (D) $V = \pm 70$ mV; (E) $V = \pm 90$ mV; (F) $V = -70$ mV. The current histograms represent the following conductive states: o, hemichannel open; c, hemichannel closed; and I = 0, zero current level. Based on o-c currents, the current histograms yielded the following conductances: 52/63 pS (positive/negative *V*) in D and 50/66 pS (positive/negative *V*) in E. (F) I_{hc} exhibits two prominent levels corresponding to $I_{hc,main}$ (bottom dotted line) and $I_{hc,residual}$ (middle dotted line). The analysis yielded the following conductances: $\gamma_{hc,main} = 62$ pS, $\gamma_{hc,residual} = 15$ pS.

The current histograms in all records show the following conductive states: O (hemichannel open), C (hemichannel closed), I = 0 (zero current level; i.e., $V_{pip} = 0$). The hemichannel closed state (C) also includes the sum of the patch leak current and membrane current. To be sure that the closed state for the hemichannel does not include any hemichannel conductance, the membrane patch conductance was investigated in cell-attached mode. It yielded a conductance of 43 ± 7 pS ($n = 8$, no open hemichannel observed). Application of CO_2 reduced it to 27 ± 5 pS (presumably by closing some membrane channels); i.e., CO_2 reduced leak/membrane current by 16 pS, which is less than hemichannel unitary conductance. In records presented here, the membrane leak conductance varies from 18 to 26 pS. Such an explanation is supported by current records exhibiting a residual state (see Fig. 3 F), which is different from the closed state, illustrated in Fig. 3 (D and E).

In Fig. 3 D, V_{pip} was stepped from 0 to 70 and then to −70 mV (i.e., *V* was made −70 and +70 mV, respectively). Fig. 3 E demonstrates a single channel at ±90 mV. In both cases, the channel opened when a positive *V* was applied and started to flicker spending most time in the main state. After inversion to a negative *V*, the channel was still apparent, but it now spent less time in the main state. The channel closure at negative voltage was voltage-dependent. At larger voltages, the channels spent less time in the main state (Fig. 3, D and E). The current histograms yielded the following conductances: 52/63 pS (positive/negative *V*) for $V = 70$ mV and 50/66 pS (positive/negative *V*) for $V = 90$ mV. In Fig. 3 F, V_{pip} was stepped from 0 to −70 mV. I_{hc} exhibited two prominent levels corresponding to $I_{hc,main}$ (bottom dotted line) and $I_{hc,residual}$ (middle dotted line). The cur-

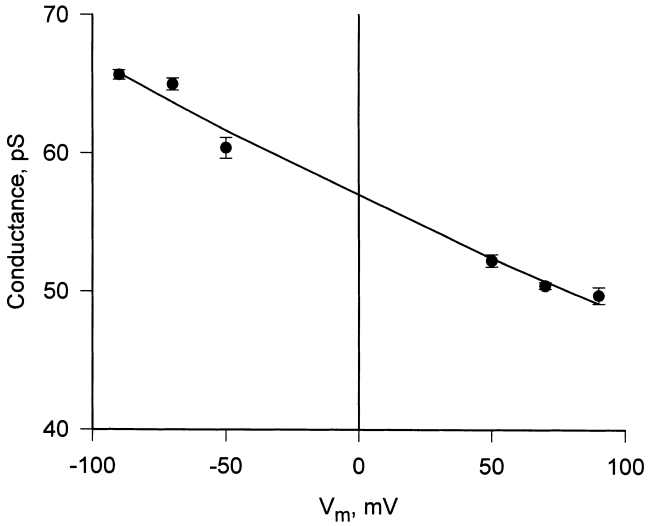

FIGURE 4. Voltage dependence of single hemichannel conductances, $\gamma_{hc,main}$. Values of $\gamma_{hc,main}$ were averaged and plotted versus V_m. Curves correspond to the best fit of data to an exponential: $\Gamma_{hc,main}$ = 57 pS at V_m = 0 mV. Symbols represent mean values ±1 SEM.

rent histogram shows that the $I_{hc,residual}$ level is different from the closed state current level. The analysis yielded the following conductances: $\gamma_{hc,main}$ = 62 pS; and $\gamma_{hc,residual}$ = 15 pS. A residual state is the property of gap junction channels and hemichannels (Bukauskas et al., 1995a; Trexler et al., 1996; Valiunas et al., 1997; Valiunas and Weingart, 2000; Oh et al., 2000).

Voltage Dependence of Single Hemichannel Conductance

The relationship between single hemichannel conductance and V_m was investigated in Cx45-HeLa cells and Cx45-RIN cells. For this purpose, $\gamma_{hc,main}$ was determined using voltage pulses of different amplitude and either polarity. The experiments were performed in Ca^{2+}-free bath solution. The data were sampled, averaged, and plotted versus V_m. Fig. 4 summarizes the results from four Cx45-HeLa cells. Similar results were obtained from Cx45-RIN cells (unpublished data). Over the voltage range examined, i.e., −90 to 90 mV, $\gamma_{hc,main}$ was dependent on V_m. It increased with hyperpolarization and decreased with depolarization. The solid curve represents the best fit of the exponential bellow to the data:

$$\gamma_{hc,\,\mathrm{main}} = \Gamma_H \cdot e^{-\frac{V}{V_H}},$$

where Γ_H corresponds to the conductance at V_m = 0 mV, and V_H is the decay constant at which $\gamma_{hc,main}$ declines to e^{-1} (Vogel and Weingart, 1998). The analysis yielded the following values: Γ_H = 57 pS and V_H = −615 mV. A gap junction channel consists of two hemichannels in series. Hence, the conductance of a gap junction channel ($\gamma_{j,main}$) can be calculated from the conductance of its hemichannels (γ_{hc1}, γ_{hc2}):

$$\gamma_{j,\,\mathrm{main}} = \frac{\gamma_{hc1,\,\mathrm{main}} \cdot \gamma_{hc2,\,\mathrm{main}}}{\gamma_{hc1,\,\mathrm{main}} + \gamma_{hc2,\,\mathrm{main}}}, \quad (1)$$

Using the values extrapolated to V = 0 mV, $\gamma_{j,main}$ was 28.5 pS. For comparison, using the same experimental conditions (22°C, pipette solution potassium aspartate [120 mM]).

$\gamma_{j,main}$ determined in pairs of Cx45-HeLa cells was 25 pS (unpublished data). A similar result (26 pS) for Cx45 was reported earlier (Veenstra et al., 1994a). These values are in good agreement with $\gamma_{j,main}$ calculated from the hemichannels data.

Open-state Probability

Cx45-HeLa cells with a single operational hemichannel also were used to study channel kinetics. The analysis of long records allowed us to explore the open-state probability (P_o) at steady state. The protocol involved the establishment of V_m gradients of different amplitude (±50, ±70, and ±90 mV) and duration (8–10 s). Current traces with one operational single hemichannel were analyzed for the dwell times in the main state. To determine P_o, the time a channel spent in the main state was measured and expressed as fraction of record duration. P_o was maximal (0.7–0.76) at positive V_m ($V_m > 50$ mV). It decreased to 0.06–0.11 when V_m was negative ($V_m < -50$ mV). This suggests that Cx45 hemichannels close in a V_m-dependent manner at negative voltage and remain open at positive V_m.

Dye Uptake Mediated by Cx45 Hemichannels

To examine the permeability properties of Cx45 hemichannels to larger molecules NT and transfected HeLa and RIN cells were incubated in bath solution (with or without 2 mM Ca^{2+}) containing 1 mg/ml LY or 2 mg/ml PI for 30 min at room temperature (22°C). Significant dye uptake occurred in the absence of external Ca^{2+}. Fig. 5 (A and C) illustrates such an experiment. The left-hand panels show phase-contrast micrographs of Cx45-HeLa and Cx45-RIN cells, respectively. Epifluorescent micrographs taken 30 min after incubation in Ca^{2+}-free bath solution containing LY showed dye uptake in Cx45-HeLa cells (Fig. 5 A) and Cx45-RIN cells (Fig. 5 C). No significant dye uptake was detected in this example in the presence of extracellular Ca^{2+} (Fig. 5, B and D). In control experiments, NT HeLa and RIN cells usually showed very little dye uptake in the presence or absence of Ca^{2+}.

Fig. 5 E summarizes the data obtained from Cx45-HeLa cells and NT HeLa cells. 85% of the Cx45-HeLa cells (n = 650) showed dye uptake in Ca^{2+}-free external solution. In the presence of 2 mM extracellular Ca^{2+}, only 1.4% of the Cx45-HeLa cells (n = 517)

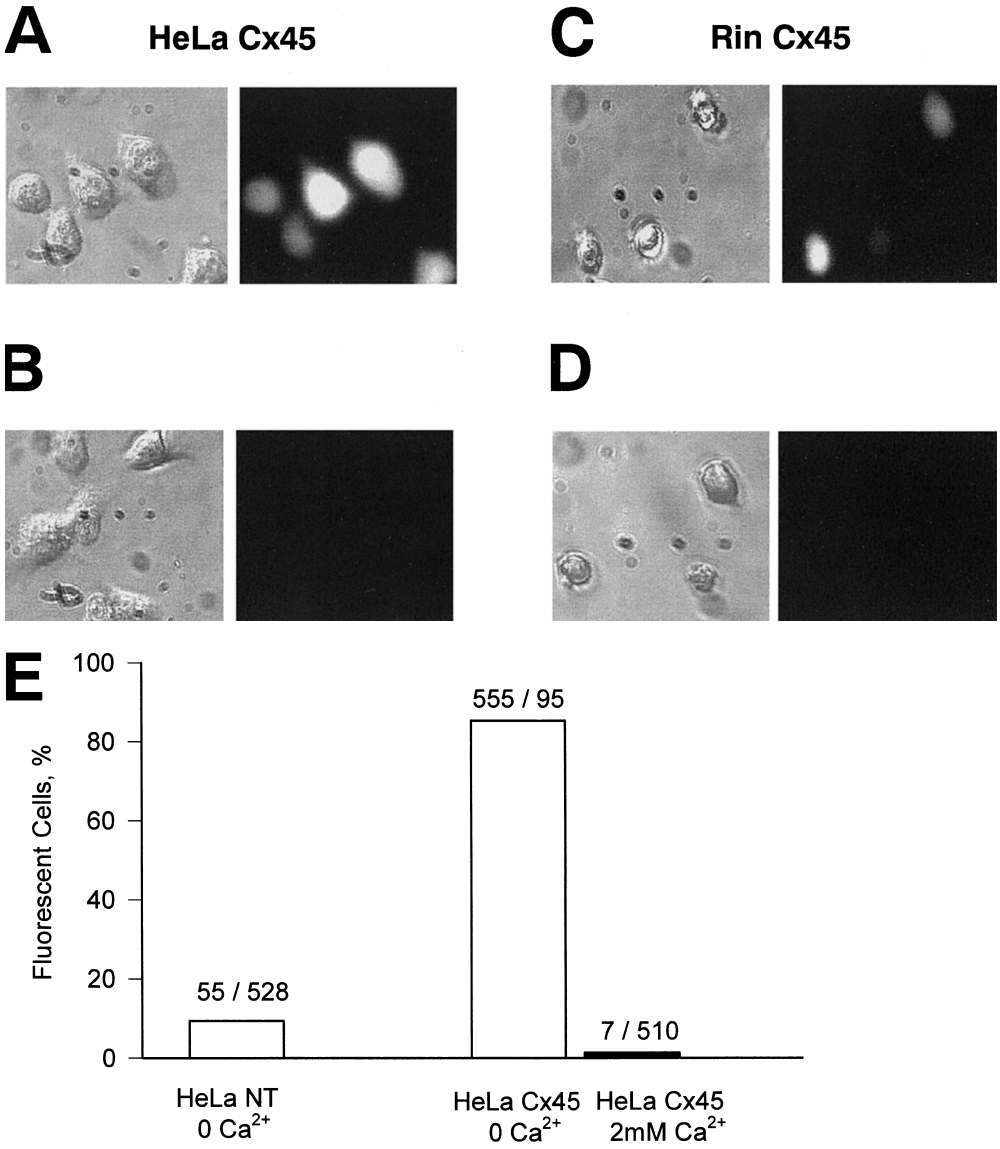

FIGURE 5. Dye uptake via Cx45 hemichannels. A-D Phase-contrast micrographs (left-hand panels) and epifluorescent micrographs (right-hand panels) taken after 30 min incubation of the cells in external solution containing LY. (A) Dye uptake by Cx45-HeLa cells in Ca^{2+}-free solution. (B) No significant dye uptake by Cx45-HeLa cells was detected in presence of 2 mM extracellular Ca^{2+}. (C) Dye uptake by Cx45-RIN cells in Ca^{2+}-free solution. (D) Similar to B, no significant dye uptake was detected by Cx45-RIN cells in the presence of 2 mM extracellular Ca^{2+}. (E) Summary of the number of cells taking up dye. 85% Cx45-HeLa cells took up dye when they were incubated with LY in Ca^{2+}-free external solution (middle bar). 1.4% of Cx45-HeLa cells (n = 517) were loaded with LY (right-hand bar) in presence of 2 mM extracellular Ca^{2+}. 9.4% of HeLa NT cells (n = 583) showed dye uptake when were bathed in Ca^{2+}-free extracellular solution. The ratio of the number of fluorescent cells to the number of nonfluorescent cells is indicated above each bar.

showed some loading with LY. 9.4% of the NT HeLa cells (n = 583) showed similar low level dye uptake when bathed in Ca^{2+}-free solution. The large difference in dye uptake between transfected and NT cells in the absence of Ca^{2+} suggests that uptake occurred through Cx45 hemichannels. The observation that dye uptake by NT HeLa cells in the absence of Ca^{2+} was larger than dye uptake by Cx45-HeLa cells in the presence of Ca^{2+} may be due to an endogenous connexin. The ratio of intensity between Cx45-HeLa cells and NT HeLa cells was large, i.e., I_{Cx45}/I_{NT} = 16.3, suggesting that expression level of endogenous connexins in NT HeLa cells is low (Eckert et al., 1993).

Induction of Dye Leak by Reduction of Extracellular Ca^{2+}

The rate of dye uptake is difficult to measure with dye in the bath. Hence, Cx45-HeLa cells that had been loaded with LY were washed with Ca^{2+}-free extracellular solution without dye and time-dependent dye unloading observed. Fig. 6 illustrates such experiments. In Fig. 6 A, the top panel shows a phase-contrast micrographs of several Cx45-HeLa cells. The epifluorescent micrographs (Fig. 6 A, middle and bottom panels), taken at 0, 30, 60, and 120 min after incubation in Ca^{2+}-free solution, show a decrease in cell fluorescence with time. Time zero (min) indicates the beginning of washout. The reduction of fluorescence intensity indicates a loss of dye into Ca^{2+}-free extracellular solution. In contrast, when LY preloaded cells were washed and bathed with external solution containing 2 mM Ca^{2+}, a marginal decrease in intensity was observed. Fig. 6 B shows epifluorescent images 0, 30, 60, and 120 min after preloading and after incubation in extracellular solution containing 2 mM Ca^{2+}. Similar results were obtained for Cx45-RIN cells (unpublished data).

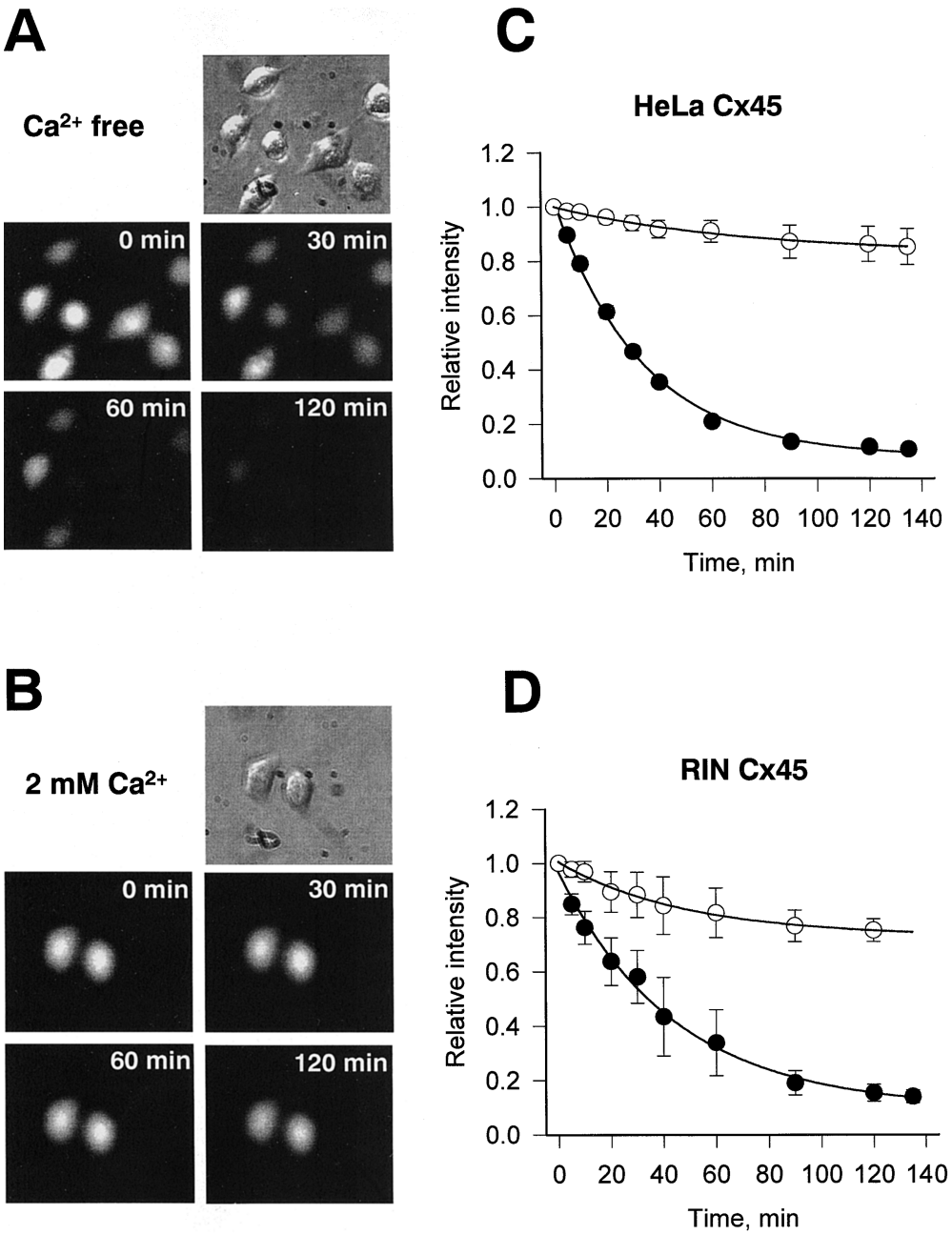

FIGURE 6. Dye leakage assays. (A) Epifluorescent micrographs (middle and bottom) taken at 0, 30, 60, and 120 min after preloading Cx45-HeLa cells with LY in Ca^{2+}-free bath solution. Time 0 min corresponds time immediately after removing LY from the bath. The reduction of fluorescence intensity with time indicates dye leak from the preloaded cells. (B) Epifluorescent images of the LY preloaded Cx45-HeLa cells at 0, 30, 60, and 120 min after removing LY from the extracellular solution which contained 2 mM Ca^{2+}. No significant decrease of fluorescence intensity was observed. (C and D) Summary of the data obtained from dye leakage experiments with Cx45-HeLa and Cx45-RIN cells. (C) Plots of normalized fluorescence intensity versus time obtained in Ca^{2+}-free (●, n = 8) and 2 mM Ca^{2+} (○, n = 5) external solution from Cx45-HeLa cells. The continuous curves represent the best fit of a single exponential to the data; Ca^{2+}-free solution: τ = 33 min, I_{min} = 0.08; 2 mM Ca^{2+}-containing solution: τ = 72 min, I_{min} = 0.85. (D) Normalized fluorescence intensity plots obtained for Cx45-RIN cells incubated with 2 mM Ca^{2+} (○, n = 3) and Ca^{2+}free (●, n = 4) bath solution. The best fit of a single exponential to data, Ca^{2+}-free solution: τ = 44 min, I_{min} = 0.09; 2 mM Ca^{2+}-containing solution: τ = 48 min, I_{min} = 0.75.

Fig. 6 (C and D) summarizes the data on dye unloading from Cx45-HeLa and Cx45-RIN cells. The fluorescence intensity was normalized, averaged, and plotted versus time. Fig. 6 C shows the results from eight Cx45-HeLa cells obtained in Ca^{2+}-free external solution (●). Over the time examined (i.e., >2 h), the intensity decreased as an exponential (smooth curve) with a time constant (τ) of 33 min to a minimum (I_{min}) corresponding to 0.08. When LY preloaded cells were incubated in Ca^{2+}-containing solution, a marginal drop of fluorescence was observed (Fig. 6 C, ○). Fitting of the data to an exponential yielded a τ of 72 min and a I_{min} of 0.85. Fig. 6 D illustrates similar results obtained with Cx45-RIN cells incubated in Ca^{2+}-containing (○) or Ca^{2+}-free (●) solution.

Concentration Dependence of Dye Uptake

A series of experiments was done to investigate the dependency of dye uptake on extracellular concentration. Cx45-HeLa cells were incubated for 30 min in external Ca^{2+}-free solution containing 0.5, 1.0, or 2 mM LY. After dye uptake, the cells were washed in external solution containing 2 mM Ca^{2+}. Fluorescence intensity at each dye concentration was measured in randomly picked cells (for 0.5 mM, n = 135 cells; for 1.0 mM, n = 218; and for 2 mM, n = 274), averaged, and plotted ver-

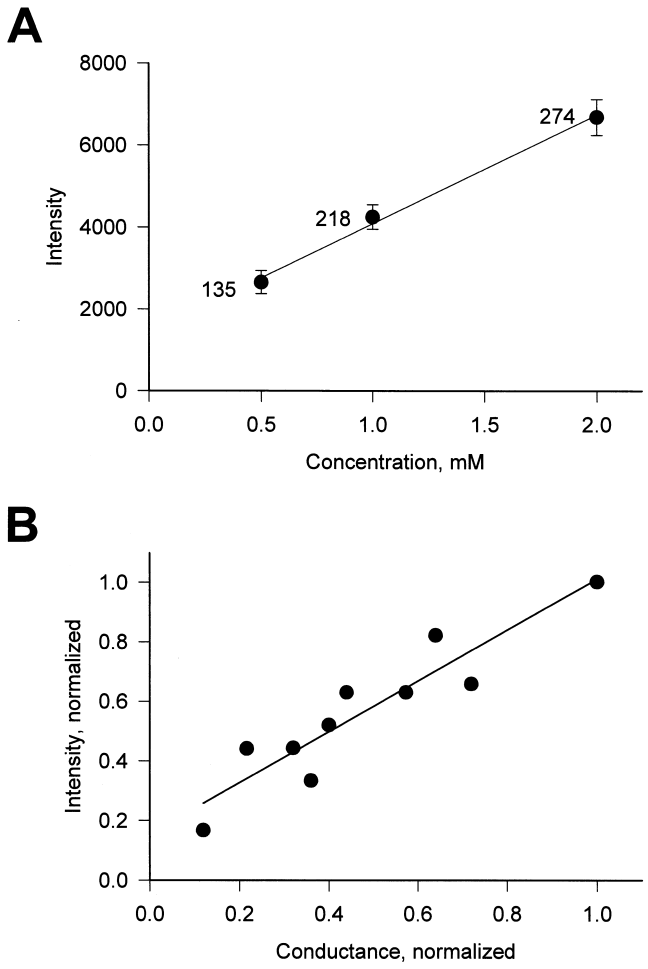

FIGURE 7. (A) The fluorescence intensity plot versus LY concentration. The continuous line represent linear relationship (r^2 = 0.995) over the range concentration investigated (i.e., 0.5–2 mM). (B) The normalized fluorescence intensity versus normalized instantaneous hemichannel conductance. The solid line corresponds to a first order regression with r^2 = 0.86.

sus concentration (Fig. 7). The fluorescence intensity increased linearly (r^2 = 0.995) over the concentration range investigated, showing no saturation at these concentrations of dye.

Dye Uptake versus Conductance

Another series of experiments was performed to investigate the correlation between dye uptake and the conductance due to functioning hemichannels. Cx45-HeLa cells were incubated in Ca^{2+}-free bath solution containing 1 mg/ml LY for 10 min at room temperature (22°C). Immediately after dye uptake, cells were washed with Ca^{2+}-free extracellular solution without dye and fluorescent images of the cells were taken. The whole-cell recording conditions were established on each of the same cells and macroscopic hemichannel currents were measured (Fig. 1 A). For each cell, $g_{hc,inst}$ and fluorescence intensity values were determined and later normalized with respect to the maximum value in the pool. Fig. 7 B shows a plot of normalized fluorescence intensity plot versus normalized instantaneous hemichannel conductance. The fluorescence intensity was directly proportional to the $g_{hc,inst}$. The solid line corresponds to a first order regression with r^2=0.86. Correlation of electrophysiological data and dye uptake demonstrates that individual cells take up dye in proportion to the number of open hemichannels.

Gap Junction Channels versus Hemichannels

The question arises whether the permeability of gap junction channels is the same as that of hemichannels and how these properties correlate with macroscopic conductances (Trexler et al., 1996). Does docking of hemichannels change the properties of the pore? Dye transfer through gap junctions was investigated using Cx45-HeLa cell pairs. LY, a negatively charged dye, was injected into one cell of a pair via patch pipette, and g_j was measured in conjunction with dye flux. Fig. 8 A illustrates an experiment demonstrating cell-to-cell spread of LY in Cx45-Hela cell pairs. The pipette containing 2 mM LY was attached in the whole-cell configuration to the left-handed cell (Fig. 8 A, cell 1; see top left-hand panel). The right-handed cell (cell 2) was patched using the perforated patch configuration. This allowed the dye spread to cell 2 without loss caused by cell dialysis via the pipette and simultaneous measurement of g_j. The epifluorescent micrographs taken at 1, 5, 10, and 30 min after dye injection in cell 1 demonstrate an increase in fluorescence in the recipient cell (Fig. 8 A). To measure g_j during dye flux, short 10-mV bipolar pulses were used to generate a transjunctional current, I_j. Fig. 8 B (left) shows the I_j at different time (5, 15, and 30 min) of the LY spread. The right panel shows a family of the voltage-dependent gap junction currents generated by series of voltage pulses (from ±10 to ±150 mV) at the 30-min time mark. The slightly asymmetric current profiles could be related to different patch configuration (cell 1, whole cell; and cell 2, perforated) and/or the influence of negatively charged LY on the voltage gate (sensor). The total g_j measured at 30 min was ~17 nS.

Fig. 8 C summarizes data gained from four dye transfer experiments. It shows a plot of fluorescence intensity versus time for injected cells (●) and moderately coupled (10–12 nS) recipient cells (O). The smooth lines correspond to the best fit of the exponential to the data. The intensity of injected cells increased to a steady state with a time constant (τ) of 5.5 min. The recipient cells filled with LY with a τ of 244.3 min. In comparison with unapposed hemichannels, the dye transfer through gap junction channels takes more time.

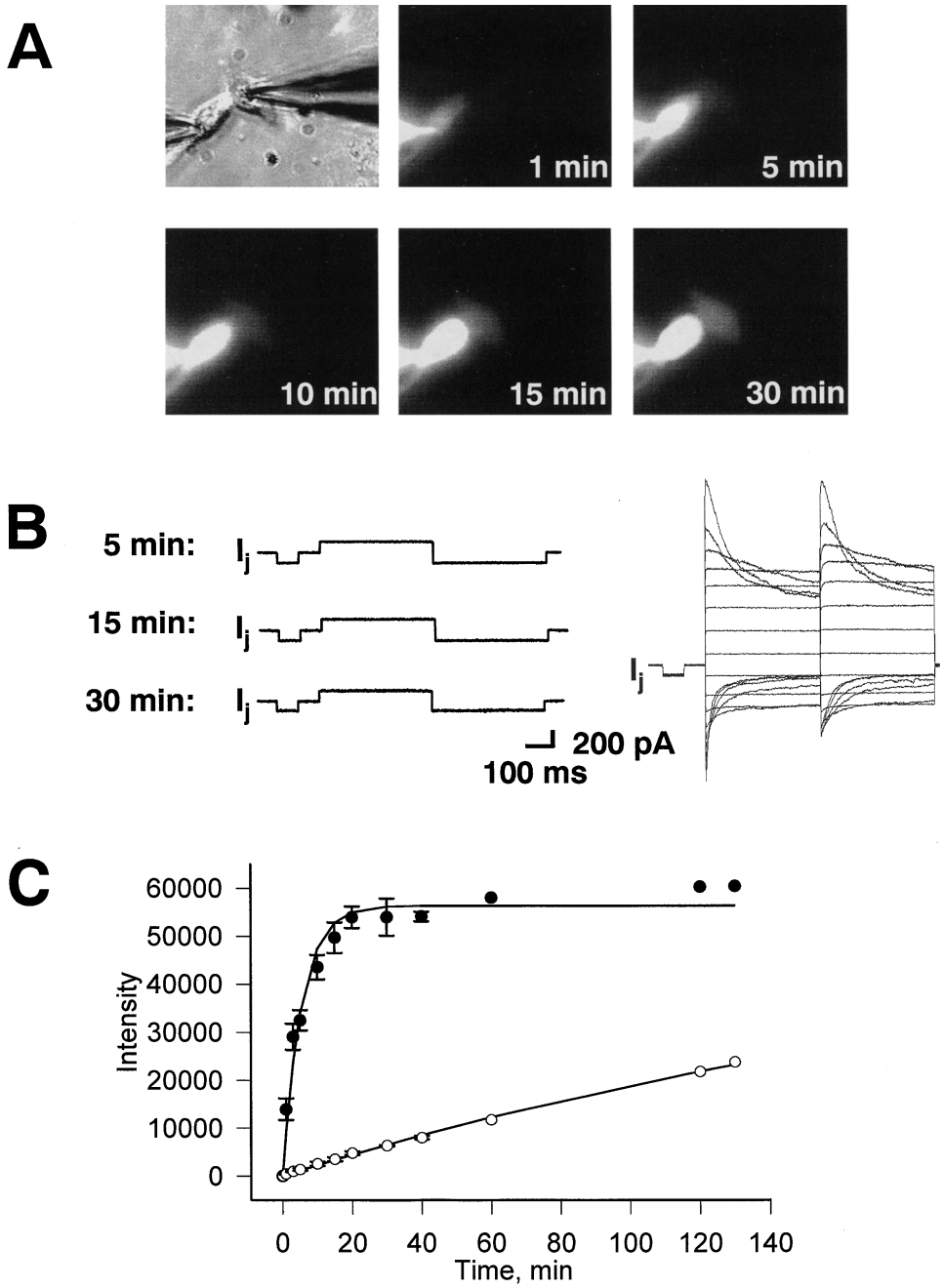

FIGURE 8. Simultaneously measurement of g_j and the dye flux between Cx45-HeLa cells. A pipette containing 2 mM LY was attached to the left-handed cell in the whole-cell configuration. The right-hand cell was patched using the perforated patch configuration. (A) Epifluorescent micrographs taken at 1 min, 5 min, 10 min and 30 min after dye injection in cell 1. Cell 2 (right-hand cell) shows fluorescence intensity increase with time. (B, left) Responses of gap junction currents to V_j gained at different times (5, 15, and 30 min) of the LY spread. Right panel shows a family of the voltage-dependent gap junction currents generated by series of voltage pulses (from ±10 to ±150 mV) at 30-min time mark. The g_j measured at 30 min was ~17 nS. (C) Quantification of cell-to-cell dye spread in Cx45-HeLa cells. Plots of fluorescence intensity versus time for injected (●) and recipient cells (○). Symbols correspond to the mean values obtained from four cell pairs. The continuous lines correspond the best fit of data to single exponentials: τ = 5.5 min for injected cells (●); τ = 244.3 min for the recipient cells (○).

Estimation of Intracellular Dye Concentration

Fluorescence intensity for injected cells reaches steady state at ~56,000 intensity units (Fig. 8 C). It is assumed that at the steady state the dye concentration within the injected cell is ~2 mM, i.e., reaches LY concentration of the patch pipette. The fluorescent intensity measured from Cx45-HeLa cells with a 30-min 2-mM LY load time in Ca^{2+}-free solution is ~6,800 (Fig. 7 A). This intensity corresponds to ~0.24 mM of LY. The data shown indicate that the total intracellular LY concentration in Cx45-HeLa cells was ~0.24 mM after 30 min of dye uptake in Ca^{2+}-free solution.

Positively Charged Dye Diffusion through Hemichannels and Gap Junction Channels

The molecules that can pass through gap junctions display a size limitation of ~1 kD (Schwarzmann et al., 1981) and junctions formed by some connexins exhibit a charge dependence (Cao et al., 1998). The dye uptake experiments described above were done using LY, which has two negative charges (MW = 457). To test whether positive charged molecules can pass through Cx45 hemichannels, 2 mg/ml propidium iodide (two positive charges, MW = 668) was used in dye uptake assays. The Cx45-HeLa and NT HeLa cells were incu-

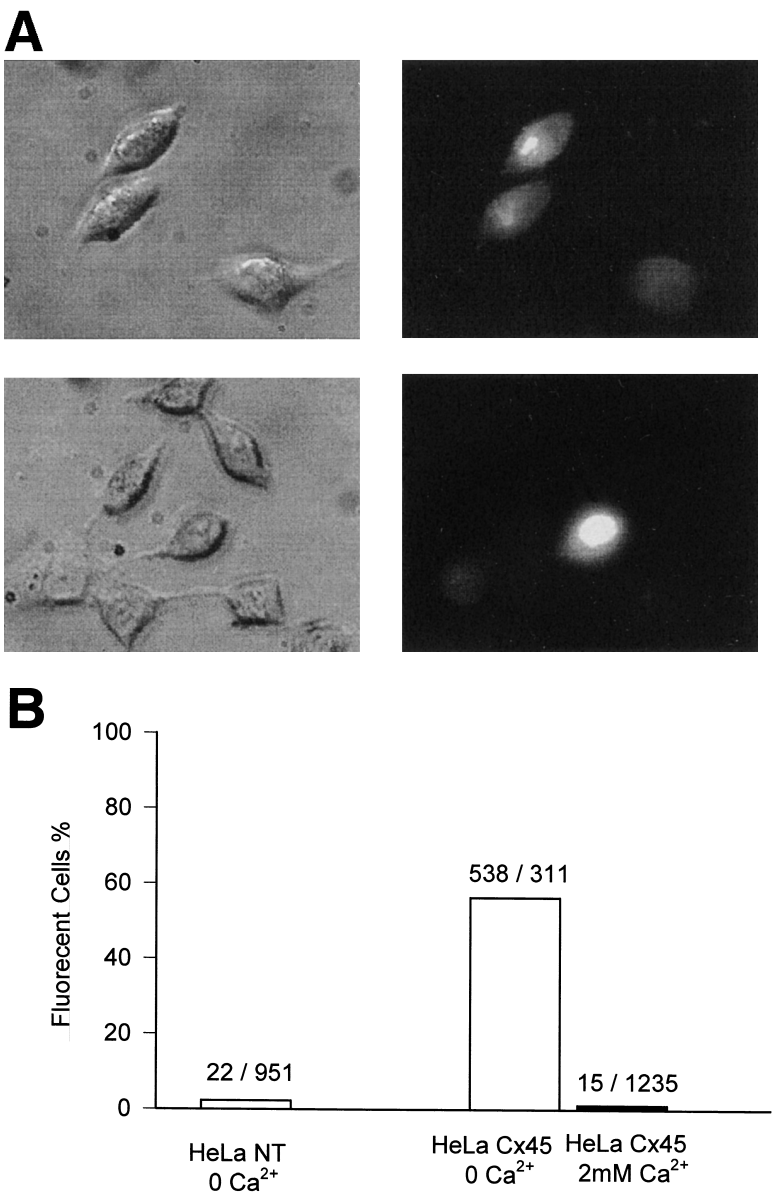

FIGURE 9. Positively charged PI uptake via Cx45 hemichannels. (A) Phase-contrast micrographs (left) and epifluorescent micrographs (right) taken after 30-min incubation of the cells in the Ca^{2+}-free external solution containing PI. Most of Cx45-HeLa cells show dye uptake. Very few Cx45-HeLa cells showed detectable dye uptake in the presence of 2 mM extracellular Ca^{2+}. (B) Summary of the number of cells taking up PI dye. 63% Cx45-HeLa cells (n = 849) showed detectable fluorescence when incubated with PI in Ca^{2+}-free external solution (middle bar). Only 1.2% of Cx45-HeLa cells (n = 1,247) were loaded with PI (right bar) in the presence of 2 mM extracellular Ca^{2+}. 2.3% of HeLa NT cells (n = 973) showed dye uptake when were bathed in Ca^{2+}-free extracellular solution. The ratio of the number of fluorescent cells to the number of nonfluorescent cells is indicated above each bar.

bated in bath solution (with 2 mM Ca^{2+} or Ca^{2+} free) containing PI for 30 min at room temperature (22°C). Only Cx45-transfected cells bathed in Ca^{2+}-free external solution sequestered PI. Fig. 9 A illustrates such an experiment. The left-hand panel shows phase-contrast micrographs of Cx45-HeLa. No significant dye uptake was detected in the presence of extracellular Ca^{2+} in Cx45-HeLa cells or nontransfected HeLa cells.

Fig. 9 B summarizes results with Cx45-HeLa cells and NT HeLa cells. Dye uptake in Ca^{2+}-free external solution occurred in 63% of the Cx45-HeLa cells (n = 849) showed. In the presence of 2 mM extracellular Ca^{2+}, only 1.2% of the Cx45-HeLa cells (n = 1,247) were loaded with PI; 2.3% of the NT HeLa cells (n = 973) showed PI uptake when bathed in Ca^{2+}-free solution. Comparison of LY data with that of PI for Cx45-HeLa cells in Ca^{2+}-free external solution shows a difference (63% for PI versus 85% for LY). Further, PI loaded Cx45-HeLa cells bathed in Ca^{2+}-free solution revealed no significant dye leak with the time in contrast to LY experiments. This could be explained by the binding of PI to DNA, negatively charged proteins, and lipids.

The PI transfer through intact gap junction channels was investigated using Cx45-HeLa cell pairs. The experimental procedure was the same as used for LY experiments. In each cell pair examined, the whole-cell recording mode was established on one cell with a dye-filled pipette. For the second cell, a gigaohm seal was established with the pipette leaving the patch intact. Dye spread into the recipient cell was recorded, then the whole-cell recording mode was established in the recipient cell and gap junction conductance (g_j) was measured. Although

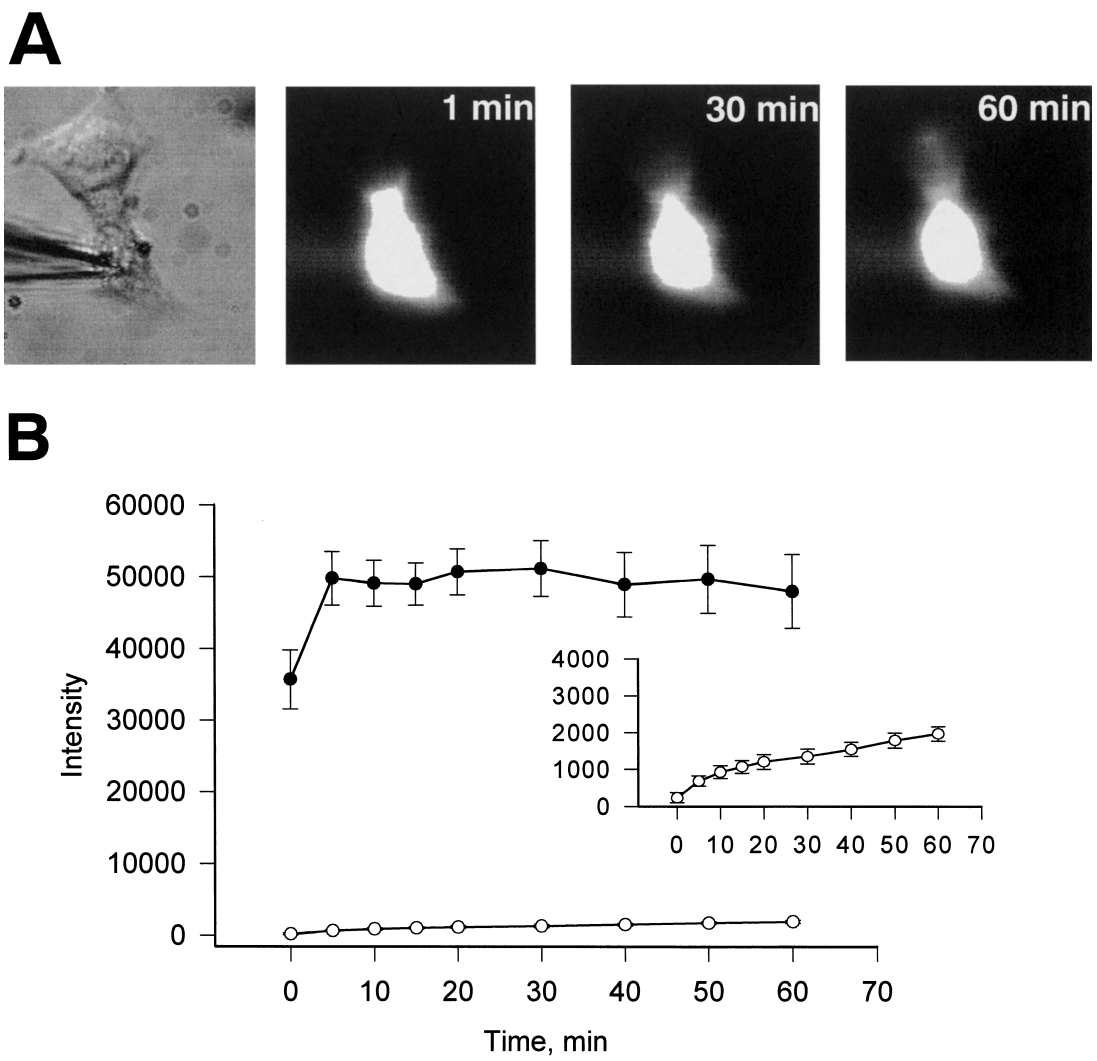

FIGURE 10. Cell-to-cell PI spread in Cx45-HeLa cells. (A) Epifluorescent micrographs taken at 1, 30, and 60 min after PI injection into cell 1 show a weak fluorescence intensity increase in recipient cell (cell 2). (B) Plots of fluorescence intensity versus time for injected cells (●) and recipient cells (○). Symbols correspond to the mean values obtained from six cell pairs. The inset illustrates recipient cells fluorescence intensity versus time on an expanded scale.

Cx45-HeLa cell pairs showed detectable PI coupling, PI diffusion was sufficiently low that it was not easily detected for a number of minutes after dye injection.

Fig. 10 shows the data from PI transfer experiments. The epifluorescent micrographs taken at 1, 30, and 60 min after PI injection in cell 1 demonstrate dye spread into the recipient cell 2 (Fig. 10 A). Fig. 10 B summarizes PI transfer data from Cx45 HeLa cell pairs ($n = 6$, $g_j =$ 6–9 nS). It shows a plot of fluorescence intensity versus time for injected cells (Fig. 10 B, ●) and the recipient cells (Fig. 10 B, ○). The inset in Fig. 10 B shows the fluorescence intensity increase in cell 2 versus time on an expanded scale. The intensity of fluorescence in the recipient cell increased very slowly over a period of 60 min, suggesting either that PI diffusion through Cx45 gap junction channels is very slow and/or PI binding is so strong that the free concentration of dye is very low and only a small amount is able to diffuse to the adjacent cell.

The data show that the quantitative analysis of PI diffusion through gap junction is complicated by PI binding effects. Quantification of the flux rates becomes very difficult. The results indicate that PI can traverse gap junctions but it is not possible to determine the flux/channel.

DISCUSSION

Hemichannel currents have been measured in *Xenopus* oocytes expressing identified connexins (for multichannel currents, rat Cx46, chicken Cx56, and *Xenopus* Cx38 [Ebihara and Steiner, 1993; Ebihara et al., 1995; Ebihara, 1996]; for single-channel currents, rat Cx46

[Trexler et al., 1996]). Recently, hemichannel currents also were recorded from human HeLa cells expressing mouse connexins Cx30, Cx46, and Cx50 (Valiunas and Weingart, 2000).

The aim of the present study has been to examine the conductance and perm-selectivity of mouse Cx45 and chicken Cx45 hemichannels in vertebrate cells and compare these properties to those of the intact gap junction channels. The electrophysiological studies in combination with dye uptake and leakage assays in the present study provide evidence for the opening of nonjunctional Cx45 hemichannels when external Ca^{2+} concentration is reduced.

Evidence for Cx45 Hemichannels

The combination of several experimental features allows the identification of Cx45 hemichannel currents. Removal of extracellular Ca^{2+} in conjunction with depolarization of V_m induced a novel current, I_{hc} (apparent in multichannel and single-channel signals) in Cx45 transfected HeLa and RIN cells, but not in nontransfected cells. This suggests that I_{hc} is carried by channels introduced by transfection, possibly Cx45 hemichannels. I_{hc} disappeared when the external Ca^{2+} was restored. This is consistent with the observation that cytosolic Ca^{2+} impairs gap junctions via chemical gating (Weingart and Bukauskas, 1995). I_{hc} in Cx45 transfected HeLa and RIN cells resembles the currents seen in *Xenopus* oocytes expressing connexins and attributed to hemichannels (Ebihara and Steiner, 1993; Ebihara et al., 1995; Trexler et al., 1996). Intracellular acidification with CO_2 caused a reversible decrease of I_{hc} in Cx45-HeLa cells (Fig. 2 A), showing that chemical gating mediated by pH changes is also a feature of Cx45 hemichannels—yet another property it shares with Cx46 hemichannels in *Xenopus* oocytes (Trexler et al., 1999). Both the pH and Ca^{2+} sensitivity of I_{hc} are consistent with the modulation of gap junction channel gating by pH and Ca^{2+} (Weingart and Bukauskas, 1995; Bukauskas and Peracchia, 1997; Francis et al., 1999). Moreover, Cx45-HeLa, and Cx45-RIN cells showed significant dye uptake in the absence of external Ca^{2+}. However, no significant dye uptake was detected in the presence of normal (2 mM) extracellular Ca^{2+}. No significant dye uptake was detected in nontransfected cells, in the presence or absence of Ca^{2+}. Thus dye transfer occurred through Cx45 hemichannels. This is consistent with studies on Cx43 (Li et al., 1996; John et al., 1999; Quist et al., 2000)

Other types of membrane channels have been identified in HeLa (two K^+ and a Cl^- channel) and RIN (BK channels) cells. These are easily distinguished from Cx45 hemichannels based on their Ca^{2+} and/or voltage sensitivity, and unitary conductance (Sauve et al., 1983, 1986; Diaz et al., 1993; Diaz and Sepulveda, 1995; Li et al., 1999).

Multichannel and Single-channel Properties

The currents of Cx45 hemichannels showed a time- and voltage-dependent deactivation or activation. I_{hc} was present at depolarized V_m. It decreased and disappeared with hyperpolarization. Gating of Cx45 hemichannels with negative V_m is expected and is consistent to the findings on other connexins (Trexler et al., 1996; Valiunas and Weingart, 2000). The slow current activation of Cx45 with positive V_m is also a typical characteristic of hemichannels (Ebihara and Steiner, 1993; Ebihara et al., 1995; Trexler et al., 1996; Valiunas and Weingart, 2000). The decline of Cx45 currents with hyperpolarization is another feature typical of hemichannels (Ebihara and Steiner, 1993; Ebihara et al., 1995).

In the present study, a key finding was that $g_{hc,ss} = f(V_m)$ of Cx45 hemichannels is S-shaped and shows no deactivation at positive V_m (Fig. 1, A and E). This suggests that voltage gating of these hemichannels is governed by negative voltage. For comparison, experiments on heterotypic gap junctions also suggested that Cx45 connexons are gated by negative V_j (Steiner and Ebihara, 1996; Valiunas et al., 2000). Earlier it was proposed that hemichannels may have two different mechanisms of voltage gating: (1) gating due to the transmembrane voltage (V_m-gating), which affects properties of cell membranes; and (2) gating, reflecting transjunctional voltage gating (V_j-gating) of gap junction channels (Trexler et al., 1996; Oh et al., 2000; Valiunas and Weingart, 2000). Hemichannel gating was studied in detail by Oh et al. (2000) in *Xenopus* oocytes expressing chimeric connexins. The authors conclude that the mechanism of V_j dependence of intercellular channels is conserved in conductive hemichannels and suggested that V_j gating results from conformational changes in individual connexin subunits.

It is interesting to note that the $g_{hc,ss}$ at $V_m = 0$ (Fig. 1 E) is ~43% of the maximum conductance at steady state for positive voltages. The time-dependent increase in hemichannel current with positive voltage steps suggests that either channel insertion occurs, or the open probability of the individual channels is increasing, or a combination of the two occur. It is probable that the P_o of Cx45 for gap junction channels at $V_j = 0$ is <1, making a combination effect most likely. Studies on the gating properties of heterotypic gap junction channels involving Cx45 connexons (i.e., Cx40-Cx45 and Cx43-Cx45; Valiunas et al., 2000; Steiner and Ebihara, 1996) are consistent with this idea: the steady-state conductance increases when the cytoplasmic side of Cx45 is positive. The $V_{m,0}$ of Cx45 is in the positive voltage range ($V_{m,0} = 11$ mV), implying that some gap junction channels involving Cx45 connexons may be closed at $V_j = 0$. The single-channel data for Cx45 collected in this study allowed us to estimate of open probability at various V_m. The P_o ranged

from 0.06 to 0.76 over a 100-mV range and yielded an estimated value of ~0.4 at $V_m = 0$ mV.

At the single-channel level, I_{hc} of Cx45 exhibited two major single-channel conductances: a main state and a residual state with short-lived substates seen occasionally (Fig. 3 F). Such a behavior was observed for Cx30 and Cx50 hemichannels in HeLa cells (Valiunas and Weingart, 2000), for Cx46 (Trexler et al., 1996) and for chimeric Cx32*Cx43 (Oh et al., 2000) hemichannels in *Xenopus oocytes* and resembles gap junction channels properties (Bukauskas et al., 1995a; Valiunas et al., 1999).

The measurements yielded a $\gamma_{hc,main} = 57$ pS for Cx45-HeLa hemichannels which can be estimated from $\gamma_{j,main}$ by means of Eq. 1. In comparison, the conductance of Cx45-HeLa gap junction channels ($\gamma_{j,main}$) was found to be 25 pS under similar ionic conditions (unpublished data). The analogous observations for Cx46 hemichannel and intact channel conductances were obtained in *Xenopus* oocytes (Trexler et al., 2000).

The unitary conductance of Cx45 hemichannels revealed a distinct V_m dependency. The $\gamma_{hc,main}$ increased with hyperpolarization and decreased with depolarization (Fig. 4). This feature has been observed earlier for other hemichannels in HeLa cells (Valiunas and Weingart, 2000) and for Cx46 hemichannels expressed in *Xenopus* oocytes (Trexler et al., 1996; Pfahnl and Dahl, 1998).

Electrophysiological studies of single and multichannel currents demonstrate the following: (1) Cx45 hemichannels are voltage-, pH-, and Ca^{2+}-gated; and (2) docking does not interfere with the polarity of gating of Cx45 gap junction channels.

Permeability Properties

Dye Uptake and Leak. Dye uptake from the external bath solution with reduced extracellular Ca^{2+} was used to assay for the opening of hemichannels. There is a strong correlation between dye uptake and Cx45 expression in the cell culture system. Cx45-transfected HeLa or RIN cells were able to sequester dye when extracellular Ca^{2+} was reduced. There was no significant dye uptake observed for NT HeLa and RIN cells (only 9.4% of NT HeLa cells took up LY versus 85% of Cx45-Hela cells). LY uptake was detected only in a small fraction of transfected cells (1.4%) in the presence of extracellular Ca^{2+}, demonstrating that extracellular Ca^{2+} plays a significant role in regulation of nonjunctional hemichannels (Ebihara and Steiner, 1993; Pfahnl and Dahl, 1999; Zampighi et al., 1999; Quist et al., 2000). Correlation of electrophysiological data and dye uptake (Fig. 7 B) demonstrated that individual cell dye uptake was in proportion to the number of open hemichannels.

The measurement of the leak of LY from preloaded cells was the principle approach in assessing hemichannel permeability properties. The fluorescent intensity of LY preloaded Cx45-transfected HeLa and RIN cells decreased markedly when incubated in Ca^{2+}-free external solution (Fig. 6). However, when LY preloaded cells were placed in solution containing 2 mM extracellular Ca^{2+}, only marginal fluorescence intensity loss was observed (~15%). The 15% loss could arise from the following: photo-bleaching effect, a small fraction of open hemichannels, or nonspecific membrane leak or efflux involving other membrane channels.

Cx45-transfected cells took up PI dye in Ca^{2+}-free external solution, suggesting that positively charged PI can pass through Cx45 hemichannels. However, in comparison to LY fewer Cx45-transfected cells absorbed PI (63% vs. 85%). This suggests that PI is less permeant than LY. Three possibilities are as follows: (1) the PI molecules are bigger than LY molecules (molecular weight of 668 vs. 457) and diffuse slower; (2) Cx45 hemichannels are selective for negative over positive charge; and (3) there is low affinity binding of PI to the hemichannel itself. Whole-cell currents obtained in Ca^{2+}-free solution from PI preloaded cells or those obtained when PI was in the patch pipette were not significantly different from nonloaded cells suggesting that if binding occurs it does not interfere with the conductive path of the hemichannel.

No detectable PI leak was observed from loaded cells even in Ca^{2+}-free solution. PI is known to localize in the nucleus and is able to bind DNA, thus reducing the free dye concentration dramatically.

Dye Diffusion through Hemichannels versus Gap Junction Channels. Dye permeation through hemichannels was qualitatively like that of gap junction channels, but the flux of dye through the hemichannel was greater than predicted based on comparison of unitary conductance for the intact gap junction channels and hemichannels. The time constant of fluorescent intensity decay ($\tau = 33$ min for Cx45-HeLa cells) obtained from dye leak experiments was 7.4-fold less than for the Cx45 gap junction channels (33 vs. 244 min). It is possible to determine the number of LY molecules passing per channel per second by taking into account the concentrations of LY within the cells. The intracellular concentration of LY in the cells exposed to 2 mM LY bathing media was 0.24 mM. The average whole cell conductance due to hemichannels was $g_{hc} = 5.94$ nS, which translates into ~104 hemichannels being open at any instance in time. The initial slope of the fluorescence intensity loss (Fig. 6 C) yields a 40% reduction in the first 20 min or an efflux of 0.09 mM. The number of molecules (MN) that efflux can be determined by: $MN = V_c \cdot \Delta C_i \cdot N_A$, where V_c is cell volume, ΔC_i is an efflux concentration, and N_A is Avogadro's number. Assuming a cell volume of 1 pl, $\sim 6.02 \times 10^7$ molecules have diffused out of the cell via the hemichannel pathway; i.e., ~434 molecules pass through each hemichannel per second (6.02×10^7/104/1,200 s = 434 molecules/channel/s). The same cal-

culation can be made for the intact gap junction channels. In this case, the concentration in the recipient cell after a 20-min exposure can be determined from Fig. 8 C. The injected cell concentration was 2 mM and the recipient cell at the 20-min mark was 0.17 mM. The average number of open channels (g_j = 10 nS) was ~400. This yields a value of 213 molecules/channel/s. Comparison of the intact channels and hemichannels permeability to LY requires normalizing the concentrations. In this case, the hemichannel concentration can be normalized to the 2 mM, concentration obtained in the pairs data. By normalizing LY concentration for the gap junction channel data and hemichannel data (about eightfold concentration increase from 0.24 to 2 mM) the difference in LY permeability can be determined. The normalized ratio for hemichannel flux to that of the gap junction channels is 3,475/213, which implies that hemichannels are 16-fold more permeable to LY than the intact gap junction channels.

There are several factors which may contribute to such a difference. In the absence of an electrical force, the ions might move independently by a random walk, for which an averaged time of $d^2/2D$ is required to diffuse a distance d (Hille, 1992), where D is diffusion coefficient. Assuming that for the intact gap junction channel distance is $>2d$, diffusion time through hemichannel should be at least four times less in comparison to gap junction channel. The hemichannel/gap junction channel flux ratio of 16 is consistent with a path length for LY in the hemichannel being about one fourth the length of the path in the gap junction channel. The difference between the conductance ratio ($\gamma_{hc,main}/\gamma_{j,main}$ = 2.28) and the LY flux ratio implies that the rate-limiting barriers/pore lengths are much more restrictive for LY than to monovalent ions in the intact gap junction channel relative to the hemichannel. It is an indication that the pore structure of the hemichannel is not merely half of a gap junction channel, but rather is significantly different than one half of an intact gap junction channel and/or the pore structure of the hemichannel is significantly different than its construct in the intact gap junction channel. For example, the hemichannel may lose the selectivity filter for LY (big charged molecules), which even in intact channel does not affect monovalent ions mobility when electrical force is applied.

Other factors that could contribute to the high hemichannel/gap junction channel permeability difference are long pore effects, such as flux coupling, flux saturation or the overcoming electrostatic barriers would result in less efficient flux of solutes (Hille, 1992). The LY binding (nonspecific, low affinity) could also affect the free pool of LY and therefore affect the hemichannel/gap junction channel permeability ratio. However, the time course for the binding of LY in the millimolar concentration range is on the order of hours (Brink and Ramanan, 1985; Ramanan and Brink, 1990) reducing the effective diffusion coefficient by a factor of 10 over a 6-h time frame, and it unlikely is an explanation for the high hemichannel/gap junction channel flux ratio.

Another possible factor which also could influence hemichannel/gap junction channel flux ratio and should be consider is the open channel probability. Under conditions where the open probability of the dye permeable channel conductance state is reduced, the time required for dye transfer could be increased. If channel substates are not permeable or less permeable to dye the flux would depend entirely upon the cumulative open time of the main state (Veenstra et al., 1994b). If open channel probability is reduced because the majority of channels are not in closed state, but in substate, the number of open channels may be overestimated from macroscopic conductance regarding to dye flux. The exact quantitatively evaluation of hemichannels and gap junction channels permeability needs further investigation.

In the case of positively charged PI, such a comparison of hemichannels and intact gap junction channels perm-selectivity is dubious because of PI binding to DNA or other negatively charged intracellular sites. Without a quantitative measure of binding (Brink and Ramanan, 1985) estimation of PI perm-selectivity is impossible. Only the qualitative statement that PI diffuses through Cx45 hemichannels or intact gap junction channels can be made.

Biological Role

This study shows that Cx45 hemichannels permit transfer of small ions as well as molecules of considerable size. This may be relevant for tissues when strong intercellular signaling and/or metabolic cooperation is involved. It is known that ischemia, hypoxia and/or other forms of metabolic inhibition contribute to cellular injury and death (Wilde and Aksnes, 1995). Recently, John et al. (1999) showed that opening of Cx43 nonjunctional hemichannels was induced by metabolic inhibition, indicating that nonjunctional hemichannels may be involved in the pathogenesis of ionic disturbances. Hemichannel activity is regulated by extracellular Ca^{2+} (Ebihara and Steiner, 1993; Pfahnl and Dahl, 1999; Valiunas and Weingart, 2000) and by membrane depolarization (De Vries and Schwartz, 1992; Ebihara et al., 1995; Trexler et al., 1996; Valiunas and Weingart, 2000). In this study, Cx45 hemichannels have been shown to open when extracellular Ca^{2+} is reduced. Membrane depolarization also is able to trigger Cx45 hemichannel opening. The large pore size of the open hemichannel may allow the flow of ions down their concentration gradients. This would result in membrane depolarization and

may be a potential arrythmogenic factor in the heart. Thus, the prevalence of Cx45 expression in the heart conductive system (Coppen et al., 1999) is consistent with this view. Reports of the putative role of hemichannels in calcium-dependent isosmotic volume regulation (Quist et al., 2000) also suggest that nonjunctional hemichannels may be physiological relevant.

The author acknowledges the expert technical assistance of Laima Valiuniene. The author would like to thank Drs. P.R. Brink and R. Weingart for advice and support, and Drs. T.W. White and R.T. Mathias for their critical comments on the manuscript. The Cx45-HeLa cells were provided by Dr. K. Willecke; parental RIN cells and Cx45-RIN cells were provided by Dr. T. Steinberg.

This work was supported by a National Institutes of Health grant (GM55263 to P.R. Brink).

Submitted: 11 June 2001
Revised: 27 December 2001
Accepted: 27 December 2001

REFERENCES

Alcolea, S., M. Theveniau-Ruissy, T. Jarry-Guichard, I. Marics, E. Tzouanacou, J.P. Chauvin, J.P. Briand, A.F. Moorman, W.H. Lamers, and D.B. Gros. 1999. Downregulation of connexin 45 gene products during mouse heart development. *Circ. Res.* 84:1365–1379.

Beblo, D.A., and R.D. Veenstra. 1997. Monovalent cation permeation through the connexin40 gap junction channel. Cs, Rb, K, Na, Li, TEA, TMA, TBA, and effects of anions Br, Cl, F, acetate, aspartate, glutamate, and NO_3. *J. Gen. Physiol.* 109:509–522.

Bevans, C.G., M. Kordel, S.K. Rhee, and A.L. Harris. 1998. Isoform composition of connexin channels determines selectivity among second messengers and uncharged molecules. *J. Biol. Chem.* 273: 2808–2816.

Beyer, E.C., and K. Willecke. 2000. Gap junctions genes and their regulation. *In* Advances in Molecular and Cell Biology. Hertzberg, E.L., editor. JAI press, Stamford, CT.

Brink, P.R., and S.V. Ramanan. 1985. A model for the diffusion of fluorescent probes in the septate giant axon of earthworm. Axoplasmic diffusion and junctional membrane permeability. *Biophys. J.* 48:299–309.

Brink, P.R., S.V. Ramanan, and G.J. Christ. 1996. Human connexin 43 gap junction channel gating: evidence for mode shifts and/or heterogeneity. *Am. J. Physiol.* 271:C321–C331.

Bruzzone, R., T.W. White, and D.L. Paul. 1996. Connections with connexins: the molecular basis of direct intercellular signaling. *Eur. J. Biochem.* 238:1–27.

Bukauskas, F.F., and C. Peracchia. 1997. Two distinct gating mechanisms in gap junction channels: CO2-sensitive and voltage-sensitive. *Biophys. J.* 72:2137–2142.

Bukauskas, F.F., C. Elfgang, K. Willecke, and R. Weingart. 1995a. Biophysical properties of gap junction channels formed by mouse connexin40 in induced pairs of transfected human HeLa cells. *Biophys. J.* 68:2289–2298.

Bukauskas, F.F., C. Elfgang, K. Willecke, and R. Weingart. 1995b. Heterotypic gap junction channels (connexin26-connexin32) violate the paradigm of unitary conductance. *Pflügers Arch.* 429:870–872.

Cao, F., R. Eckert, C. Elfgang, J.M. Nitsche, S.A. Snyder, D.F. Hulser, K. Willecke, and B.J. Nicholson. 1998. A quantitative analysis of connexin-specific permeability differences of gap junctions expressed in HeLa transfectants and *Xenopus* oocytes. *J. Cell Sci.* 111:31–43.

Coppen, S.R., I. Kodama, M.R. Boyett, H. Dobrzynski, Y. Takagishi, H. Honjo, H.I. Yeh, and N.J. Severs. 1999. Connexin45, a major connexin of the rabbit sinoatrial node, is co-expressed with connexin43 in a restricted zone at the nodal-crista terminalis border. *J. Histochem. Cytochem.* 47:907–918.

Davis, L.M., H.L. Kanter, E.C. Beyer, and J.E. Saffitz. 1994. Distinct gap junction protein phenotypes in cardiac tissues with disparate conduction properties. *J. Am. Coll. Cardiol.* 24:1124–1132.

De Vries, V.S., and E.A. Schwartz. 1992. Hemi-gap-junction channels in solitary horizontal cells of the catfish retina. *J. Physiol.* 445: 201–230.

Diaz, M., and F.V. Sepulveda. 1995. Characterisation of $Ca^{(2+)}$-dependent inwardly rectifying K^+ currents in HeLa cells. *Pflügers Arch.* 430:168–180.

Diaz, M., M.A. Valverde, C.F. Higgins, C. Rucareanu, and F.V. Sepulveda. 1993. Volume-activated chloride channels in HeLa cells are blocked by verapamil and dideoxyforskolin. *Pflügers Arch.* 422:347–353.

Ebihara, L. 1996. Xenopus connexin38 forms hemi-gap-junctional channels in the nonjunctional plasma membrane of Xenopus oocytes. *Biophys. J.* 71:742–748.

Ebihara, L., and E. Steiner. 1993. Properties of a nonjunctional current expressed from a rat connexin46 cDNA in Xenopus oocytes. *J. Gen. Physiol.* 102:59–74.

Ebihara, L., V.M. Berthoud, and E.C. Beyer. 1995. Distinct behavior of connexin56 and connexin46 gap junctional channels can be predicted from the behavior of their hemi-gap-junctional channels. *Biophys. J.* 68:1796–1803.

Eckert, R., A. Dunina-Barkovskaya, and D.F. Hulser. 1993. Biophysical characterization of gap-junction channels in HeLa cells. *Pflügers Arch.* 424:335–342.

Evans, W.H., S. Ahmed, J. Diez, C.H. George, J.M. Kendall, and P.E.M. Martin. 1999. Trafficking pathways leading to the formation of gap junctions. *In* Novartis Foundation 219. Gap junction mediated intercellular signalling in health and disease. Wiley, New York. 44-54.

Fan, J.S., and P. Palade. 1998. Perforated patch recording with beta-escin. *Pflügers Arch.* 436:1021–1023.

Foote, C.I., L. Zhou, X. Zhu, and B.J. Nicholson. 1998. The pattern of disulfide linkages in the extracellular loop regions of connexin 32 suggests a model for the docking interface of gap junctions. *J. Cell Biol.* 140:1187–1197.

Francis, D., K. Stergiopoulos, J.F. Ek-Vitorin, F.L. Cao, S.M. Taffet, and M. Delmar. 1999. Connexin diversity and gap junction regulation by pHi. *Dev. Genet.* 24:123–136.

Hille, B. 1992. Ionic Channels of Excitable Membranes. 2nd ed. Sinauer Associates, Inc., Sunderland, MA. 607 pp.

John, S.A., R. Kondo, S.Y. Wang, J.I. Goldhaber, and J.N. Weiss. 1999. Connexin-43 hemichannels opened by metabolic inhibition. *J. Biol. Chem.* 274:236–240.

Kanter, H.L., J.G. Laing, S.L. Beau, E.C. Beyer, and J.E. Saffitz. 1993. Distinct patterns of connexin expression in canine Purkinje fibers and ventricular muscle. *Circ. Res.* 72:1124–1131.

Krisciukaitis, A. 1997. Computer programs for investigation of intercellular communication using double whole-cell voltage clamp. *Electron Elect. Eng.* 4:71–83.

Li, H., T.F. Liu, A. Lazrak, C. Peracchia, G.S. Goldberg, P.D. Lampe, and R.G. Johnson. 1996. Properties and regulation of gap junctional hemichannels in the plasma membranes of cultured cells. *J. Cell Biol.* 134:1019–1030.

Li, Z.W., J.P. Ding, V. Kalyanaraman, and C.J. Lingle. 1999. RINm5f cells express inactivating BK channels whereas HIT cells express noninactivating BK channels. *J. Neurophysiol.* 81:611–624.

Malchow, R.P., H. Qian, and H. Ripps. 1993. Evidence for hemi-gap

junctional channels in isolated horizontal cells of the skate retina. *J. Neurosci. Res.* 35:237–245.

Oh, S., C.K. Abrams, V.K. Verselis, and T.A. Bargiello. 2000. Stoichiometry of transjunctional voltage-gating polarity reversal by a negative charge substitution in the amino terminus of a connexin32 chimera. *J. Gen. Physiol.* 116:13–31.

Pfahnl, A., and G. Dahl. 1998. Localization of a voltage gate in connexin46 gap junction hemichannels. *Biophys. J.* 75:2323–2331.

Pfahnl, A., and G. Dahl. 1999. Gating of cx46 gap junction hemichannels by calcium and voltage. *Pflügers Arch.* 437:345–353.

Quist, A.P., S.K. Rhee, H. Lin, and R. Lal. 2000. Physiological role of gap-junctional hemichannels. Extracellular calcium-dependent isosmotic volume regulation. *J. Cell Biol.* 148:1063–1074. Ramanan, S.V., and P.R. Brink. 1990. Exact solution of a model of diffusion in an infinite chain or monolayer of cells coupled by gap junctions. *Biophys. J.* 58:631–639.

Ramanan, S.V., and P.R. Brink. 1990. Exact solution of a model diffusion in an infinite chain or monolayer of cells coupled by gap junctions. *Biophys. J.* 58:631–639.

Saez, J.C., J.A. Connor, D.C. Spray, and M.V. Bennett. 1989. Hepatocyte gap junctions are permeable to the second messenger, inositol 1,4,5-trisphosphate, and to calcium ions. *Proc. Natl. Acad. Sci. USA.* 86:2708–2712.

Saffitz, J.E., H.L. Kanter, K.G. Green, T.K. Tolley, and E.C. Beyer. 1994. Tissue-specific determinants of anisotropic conduction velocity in canine atrial and ventricular myocardium. *Circ. Res.* 74: 1065–1070.

Sauve, R., G. Roy, and D. Payet. 1983. Single channel K+ currents from HeLa cells. *J. Membr. Biol.* 74:41–49.

Sauve, R., C. Simoneau, R. Monette, and G. Roy. 1986. Single-channel analysis of the potassium permeability in HeLa cancer cells: evidence for a calcium-activated potassium channel of small unitary conductance. *J. Membr. Biol.* 92:269–282.

Schwarzmann, G., H. Wiegandt, B. Rose, A. Zimmerman, D. Ben-Haim, and W.R. Loewenstein. 1981. Diameter of the cell-to-cell junctional membrane channels as probed with neutral molecules. *Science.* 213:551–553.

Steiner, E., and L. Ebihara. 1996. Functional characterization of canine connexin45. *J. Membr. Biol.* 150:153–161.

Trexler, E.B., M.V. Bennett, T.A. Bargiello, and V.K. Verselis. 1996. Voltage gating and permeation in a gap junction hemichannel. *Proc. Natl. Acad. Sci. USA.* 93:5836–5841.

Trexler, E.B., F.F. Bukauskas, M.V. Bennett, T.A. Bargiello, and V.K. Verselis. 1999. Rapid and direct effects of pH on connexins revealed by the connexin46 hemichannel preparation. *J. Gen. Physiol.* 113:721–742.

Trexler, E.B., F.F. Bukauskas, J. Kronengold, T.A. Bargiello, and V.K. Verselis. 2000. The first extracellular loop domain is a major determinant of charge selectivity in connexin46 channels. *Biophys. J.* 79:3036–3051.

Valiunas, V., and R. Weingart. 2000. Electrical properties of gap junction hemichannels identified in transfected HeLa cells. *Pflügers Arch.* 440:366–379.

Valiunas, V., F.F. Bukauskas, and R. Weingart. 1997. Conductances and selective permeability of connexin43 gap junction channels examined in neonatal rat heart cells. *Circ. Res.* 80:708–719.

Valiunas, V., D. Manthey, R. Vogel, K. Willecke, and R. Weingart. 1999. Biophysical properties of mouse connexin30 gap junction channels studied in transfected human HeLa cells. *J. Physiol.* 519: 631–644.

Valiunas, V., R. Weingart, and P.R. Brink. 2000. Formation of heterotypic gap junction channels by connexins 40 and 43. *Circ. Res.* 86:E42–E49.

Vaney, D.I., J.C. Nelson, and D.V. Pow. 1998. Neurotransmitter coupling through gap junctions in the retina. *J. Neurosci.* 18:10594–10602.

Veenstra, R.D., H.Z. Wang, E.C. Beyer, and P.R. Brink. 1994a. Selective dye and ionic permeability of gap junction channels formed by connexin45. *Circ. Res.* 75:483–490.

Veenstra, R.D., H.Z. Wang, E.C. Beyer, S.V. Ramanan, and P.R. Brink. 1994b. Connexin37 forms high conductance channels with subconductance state activity and selective dye and ionic permeabilities. *Biophys. J.* 66:1915–1928.

Veenstra, R.D., H.Z. Wang, D.A. Beblo, M.G. Chilton, A.L. Harris, E.C. Beyer, and P.R. Brink. 1995. Selectivity of connexin-specific gap junctions does not correlate with channel conductance. *Circ. Res.* 77:1156–1165.

Vogel, R., and R. Weingart. 1998. Mathematical model of vertebrate gap junctions derived from electrical measurements on homotypic and heterotypic channels. *J. Physiol. (Lond.).* 510:177–189.

Wang, H.Z., and R.D. Veenstra. 1997. Monovalent ion selectivity sequences of the rat connexin43 gap junction channel. *J. Gen. Physiol.* 109:491–507.

Weingart, R., and F.F. Bukauskas. 1995. Regulation of gap junctions by liphophilic agents and ions supports the concept of two gating mechanisms. *Experientia.* 51:A68. (Abstr.)

Wilde, A.A., and G. Aksnes. 1995. Myocardial potassium loss and cell depolarisation in ischaemia and hypoxia. *Cardiovasc. Res.* 29:1–15.

Zampighi, G.A., D.D. Loo, M. Kreman, S. Eskandari, and E.M. Wright. 1999. Functional and morphological correlates of connexin50 expressed in *Xenopus laevis* oocytes. *J. Gen. Physiol.* 113:507–524.